INVESTIGATION OF A GRID INDUCED TURBULENT ENVIRONMENT FOR WIND TUNNEL TESTING

by

Timothy Allen Reinhold

Thesis submitted to the Graduate Faculty of the
Virginia Polytechnic Institute and State University
in partial fulfillment of the requirements for the degree of
MASTER OF SCIENCE
in
Engineering Science and Mechanics

APPROVED:

F. J. Maher, Chairman

H. W. Tieleman

A. W. Bennett

February, 1975

Blacksburg, Virginia

ACKNOWLEDGEMENTS

The author wishes to acknowledge the contributions of Professors Frank J. Maher, Henry W. Tieleman and Archie W. Bennett and the financial assistance given by the National Science Foundation through the grant GK 35801.

A special word of appreciation is extended to Professors Maher and Tieleman for their suggestions, criticism and adivce throughout the course of this study and the preparation of this paper.

Acknowledgement is also made of the help obtained during the testing phase of this study, from Mr. Alexander Robert Sadlowe, a student assistant and Mr. Harry Dawson the wind tunnel technician.

CONTENTS

LIST OF ILLUSTRATIONS

LIST OF ILLUSTRATIONS IN APPENDICES

LIST OF SYMBOLS

b Bar Width of Grid

f Frequency, Hz

G(n) One Sided Power Spectral Density Function

$$= 4\int_0^\infty R(\tau)\cos(2\pi f\tau)d\tau$$

$\hat{G}(n)$ Estimate of the One Sided Power Spectral Density Function

$$= 4\int_0^\infty \omega(\tau)\, R(\tau)\cos(2\pi f\tau)d\tau$$

L Integral Length Scale

$$\int_0^\infty R(l)dl$$

l Displacement Usually Given As: x, y or z

M Mesh Size of Grid

n Frequency, Hz

R(l) Correlation Coefficient for Velocity Components at Two Different Points in Space but at the Same Instant in Time

$$= \frac{\overline{u_1' u_2'}}{\sqrt{\overline{u_1^2}}\sqrt{\overline{u_2^2}}}$$

$R(\tau)$ Autocovariance Coefficient $= \overline{u_1'(t)\, u_1'(t-\tau)}$

$R'(\tau)$ Normalized Autocovariance Coefficient

$$= \frac{\overline{u_1'(t)\, u_1'(t-\tau)}}{\overline{u_1^2}}$$

$S(n)$	Two Sided Power Spectral Density Function $= \int_{-\infty}^{\infty} R(\tau) \cos (2\pi f\tau) d\tau$
$\hat{S}(n)$	Estimate of Two Sided Power Spectral Density Function $= \int_{-\infty}^{\infty} \omega(\tau) R(\tau) \cos (2\pi f\tau) d\tau$
T_m	Maximum Delay Time $= \tau_m$
t	Time
u	Velocity
$\bar{u}$	Mean Velocity
u'	Fluctuating Velocity Component
$\overline{u^2}$	Variance of Fluctuating Velocity Component
$\sqrt{\overline{u^2}}/\bar{u}$	Turbulence Intensity
x	Distance Downstream of Grid
xyz	Subscripts Denoting Direction in Cartesian Grid Coordinate System - Figure 1
$\Phi(n)$	Normalized One Sided Power Spectral Density Function $= \frac{G(n)}{\overline{u^2}}$
τ	Lag Time or Delay Time

INTRODUCTION

Engineers have been concerned about the effects of natural winds on structures for many generations. As a result, wind tunnel testing of models to obtain data for the design of structures has become a widely used technique. However, most modeling schemes of the past decades have involved wind tunnel testing under smooth flow conditions. Recently, as full scale data have become available, investigators have attempted to simulate the turbulence of natural winds in wind tunnel tests. Obstructions, generally in the form of a coarse grid along with a boundary layer trip have been mounted in tunnel throats and the properties of the turbulence generated have been measured at various locations downstream of the obstruction. The obstructions are designed and oriented so that the velocity profile and turbulence intensity produced at the model location are similar to those expected at the site of the actual structure. Ideally, the exact character of the expected natural wind should be modeled in wind tunnel investigations of proposed structures. At present, most of the characteristics of the natural turbulent winds which have been measured can be modeled in the wind tunnel within reasonable limits. Two notable exceptions are the scale of the turbulence and short time variations in winds due to the passage of squall lines, thunderstorms and the like. Consequently, it is important that current experimental investigations performed in wind tunnels should include tests with both smooth and turbulent flows. The results should indicate whether the structural loading or response may be altered due to the presence of turbulence. The scale of turbulence

produced in the wind tunnel with present methods is too small for reasonably sized models to be used. Vickery (1) indicates that, with some caution, turbulence, produced by an obstruction in the form of a coarse grid, in a 7 foot by 7 foot wind tunnel can be used to study the loading of structures with a scale of about 400:1. In order to measure surface pressures or to investigate the wake characteristics of structures in any detail, larger models are desirable. The technology necessary to produce high intensity turbulence with integral length scales large enough to allow the use of larger models, in most aerodynamic wind tunnels, is not yet available. It is believed that some idea of the effects of turbulence on the response of structures can be obtained from wind tunnel tests in turbulent flows even though the integral length scales are not large enough to adequately model atmospheric turbulence.

For the special case of a structure which is high above the ground and much longer in one direction than in the other two, the use of a two dimensional flow field would seem appropriate. Structures which fit this description include long suspension bridges which clear the water level by 150 feet or more at their center. For a bridge with a depth of 25 feet at a height of 150 feet, the variation in mean velocity across the depth of the bridge is 4.8% if the velocity profile has a power law exponent of 0.4 and only 2.4% if the velocity profile has a power law exponent of 0.16. The most likely case for excitation would be for wind flowing normal to the bridge, and parallel to the water surface, for which the power law exponent of the velocity profile

is probably close to 0.16. The turbulence intensity and the structure of the turbulence are likewise almost invariant across the depth of the bridge. Consequently, modeling of suspension bridges, which fit the above criterion, can be performed in a turbulent flow which is uniform across the tunnel cross-section. Such a turbulent flow is readily produced by a uniform coarse grid.

As a result of the desire to use both smooth and turbulent flows in wind tunnel studies modeling suspension bridges which meet the criteria outlined above, a uniform coarse grid was designed and built for use in the VPI & SU 6 foot by 6 foot wind tunnel. This report presents a description of the turbulent flows subsequently generated for use in model studies. Figure (1) shows the grid design and indicates the axes to be used in locating points behind the grid.

DESCRIPTION OF WIND TUNNEL FLOW CONDITIONS

The Smooth Flow

The VPI & SU wind tunnel is an extremely low turbulence closed return tunnel. At the maximum velocity used in these tests of 100 feet per second, the wind fluctuations caused voltage variations in the output of a hot wire anemometer which were on the order of two millivolts. This is interpreted as a turbulence intensity measurement on the order of 0.10 percent.

The Turbulent Flow

Numerous investigations have been made which seek to determine the characteristics of turbulence behind a uniform coarse grid. Empirical and semi-empirical relationships have been proposed which would predict the statistical and mean properties of the flow to aid in selecting a type of grid and in designing its characteristic dimensions. One of the earliest investigations was by H. L. Dryden, G. B. Schubauer and others in 1937 (2). They measured scales and intensities for a variety of mesh and bar sizes and proposed semi-empirical relations for each utilizing the mesh size (M) as the reference length. In 1951, Baines and Peterson (3) indicated that the bar size (b) rather than the mesh size is the more important reference length in describing the decay of grid turbulence. They proposed that the turbulence intensity in the region of isotropic turbulence decay can be represented by the following approximate relationship

$$\frac{\sqrt{\overline{u^2}}}{\overline{u}} = 1.12 \left(\frac{x}{b}\right)^{-5/7} \quad . \tag{1}$$

The measurements of scales in the above articles were performed by measuring the correlation coefficient between the signals of two hot wire anemometer probes at varying lateral separation and using the definition,

$$L_y \equiv \int_0^\infty R(y)dy \tag{2}$$

Baines and Peterson (3) measured values of scale and intensity which are within the experimental scatter of values measured by Dryden et al (2).

Analysis of grid turbulence by analytic techniques has also attracted a great deal of interest. The interest arises from the fact that grid turbulence, after an initial generation period, approaches the conditions of decaying isotropic turbulence. For conditions of decaying isotropic turbulence, a mathematical formulation for the flow has been developed by Taylor (4) and von Karman (5) which predicts some possible relations for large Reynold number flows. For isotropic turbulence, the two integral length scales transverse to the flow direction are equal and half as large as the longitudinal integral length scale. For flows with large Reynold's numbers, it is predicted that the turbulence intensity and integral length scales measured at a specific distance downstream of the grid are independent of the wind velocity. Von Karman (5) predicts that the integral length scale will be a function of (M) and ($\overline{u}t/M$) where "t" is decay time and $\overline{u}$ is the

free stream velocity. He further states that in the case of "self-preserving" turbulence the fundamental relation will be some power of $(\bar{u}t/M)$. Self-preservation is used to refer to a turbulent flow for which the structure of the eddies is similar, when properly scaled, throughout the decay of the turbulence.

Several problems arise in attempting to verify the analytical expressions experimentally. The bounds of the region where isotropic turbulence can be assumed are unclear and the magnitudes of the Reynold's number for which Taylor's (4) and von Karman's (5) relations are valid are not listed. For example, Marshall (6) found that at a distance of eight mesh lengths downstream of the grid, the longitudinal integral length scale was 2.5 times larger than the lateral integral length scale. Stewart and Townsend (7) indicate that a significant proportion of the total turbulent energy may be in eddies which are not self-preserving in nature.

Several investigators, since Dryden and Baines and Peterson, have measured turbulence intensities and scales behind grids leading to different empirical relations. Vickery (1) added his data for lateral integral length scales to that of Baines and Peterson (3) but chose a curve with a significantly different slope, than that used by Baines and Peterson, as his trend for the variation of scale downstream of the grid. Most of the older measurements of scales contain so much scatter in values that it is not difficult to draw curves which represent the trends of the data but have radically different slopes. Walshe (8) quotes Whitbread as proposing the following tentative rela-

tionship for turbulence intensity variation behind a grid

$$\frac{\sqrt{\overline{u^2}}}{\overline{u}} = 3.27 \left(\frac{x}{b}\right)^{-0.955} \quad . \tag{3}$$

It should be noted that Whitbread's relation for turbulence intensity predicts much higher levels of turbulence than the Baines and Peterson relation. These higher values are closer to those measured in this study as well as to those measured by Vickery (1) in 1965, by Marshall (6) in 1968 and by Laneville and Parkinson (9) in 1971. A number of these measurements are represented in Figure (2). The magnitude of the turbulence intensity measured has risen significantly in recent years; possibly due in part to better equipment and shorter length hot wires. A further explanation for the scatter, at least for displacements less than twelve mesh lengths downstream of the grid, may be due to the variation of intensity measured behind a bar as opposed to that behind a mesh opening. Marshall (6) shows this difference quite clearly and his results are reproduced in Figure (3). The value of the exponent in equation (3) may even be dependent on the ratio of bar size to mesh size.

In view of the variation in measurements of different investigators, it was decided to perform a limited study of the particular grid used to generate a uniform turbulent flow in the VPI & SU stability wind tunnel. Values of scales and intensities of the turbulence as well as the power spectral density function of the longitudinal velocity component were determined at various points downstream of the grid.

The Grid

The turbulence grid used in the VPI & SU wind tunnel was built with the same ratio of sizes as the grid used by Vickery (1). Both the mesh size to bar width ratio and the mesh size to tunnel width ratio are identical to those used in Vickery's grid. The mesh size is 18 inches which is one-fourth the width of the tunnel and the bar size was 3.6 inches. This results in a bar size to mesh size ratio of 0.2. Figure (1) shows the grid and the axes used to locate points in the flow.

Uniformity of the Flow

The uniformity of the flow across the tunnel cross-section was studied at four locations downstream of the grid. The locations were at x/b equal to 38.33, 44.44, 52.92 and 61.25. The results are shown in Figure (4) and give the maximum variations at 38.33 bar widths downstream of the grid to be 3% for the mean velocity and 4% for the average turbulence intensity. The percentage variation in the turbulence intensity is defined to be the difference between the turbulence intensity measured at a point and the average of the intensities measured at that cross-section divided by the average intensity measured at that cross-section. Farther downstream the maximum variation of the mean velocity was about 2.5%. The maximum variation of the turbulence intensity from the average value at the given cross-section was about 3% for distances greater than 40 bar widths downstream of the grid. These results are consistent with those measured by Vickery (1), Marhsall (6) and Laneville (9). Measurements of inte-

gral length scales and power spectral density estimates were also found to be uniform across the tunnel cross-section for distances greater than 35 bar widths downstream of the grid.

Turbulence Intensities and Integral Length Scales

Turbulence intensities and integral length scales of the longitudinal velocity component were measured at 9 positions downstream of the grid for flows with mean velocities of about 40, 60, and 80 feet per second. The positions were located 5 bar widths apart beginning at 30 bar widths downstream of the grid and progressing in the downstream direction.

The turbulence intensity measurements are shown in Figure (5). There is a little scatter in the data but nothing systematic enough to indicate a variation of the turbulence intensity with velocity. The fact that the turbulence intensity is independent of velocity is further shown in Figure (6) where the intensity is plotted for seven different velocities at a distance of 8 mesh lengths or 40 bar widths downstream of the grid. The values of turbulence intensity measured agreed well with Marshall's results (6) as shown in Figure (3) and were only slightly higher than the values measured by Laneville (9) as shown in Figure (2). Further, the data in Figure (5) was fit, by the method of least squares, to an expression similar to the one used by Baines and Peterson and Whitbread. The resulting empirical expression, also shown in Figure (5), is:

$$\frac{\sqrt{\overline{u^2}}}{\overline{u}} = 4.57 \left(\frac{x}{b}\right)^{-1} \quad . \tag{4}$$

The range of distances downstream of the grid for which this expression is valid can be estimated from the trends in Figure (2). The expression should be valid for (x/b) greater than 25 but less than 150. Whitbread's relation, equation (3) is quite similar to the present expression.

The values for the longitudinal integral length scales are shown in Figure (7). The open data markers represent the scale as calculated from the area under the autocorrelation curve. These are computed using the definition

$$L_x \equiv \int_0^\infty R(x)dx \tag{5.1}$$

and applying Taylor's hypothesis,

$$L_x = \overline{u}_x \int_0^\infty R_x'(\tau)d\tau \quad . \tag{5.2}$$

The solid data markers represent the values of the integral length scale predicted by the value of the power spectral density function at zero frequency $G_x(0)$. The autocorrelation function and the power spectral density function are Fourier transforms of each other

$$R_x(\tau) = \int_0^\infty G_x(f) \cos (2\pi f\tau)df \tag{6.1}$$

$$G_x(f) = 4\int_0^\infty R_x(\tau) \cos (2\pi f\tau)d\tau \quad . \tag{6.2}$$

For f = 0,

$$G_x(0) = 4\int_0^\infty R_x(\tau)d\tau = 4\,\overline{u^2}\int_0^\infty R_x'(\tau)d\tau \tag{6.3}$$

therefore from the above relation for L_x,

$$L_x = \frac{G_x(0)\overline{u}_x}{4\overline{u_x^2}} \quad . \tag{6.4}$$

The values of the longitudinal integral length scales are plotted for three different mean velocities. The data suggests a definite increase in the integral length scale with increased velocity and a growth in scale as the turbulence decays. Other experimenters, Dryden (2) and Bearman (10) state that they have found no variation in scale corresponding to a variation in velocity. All the experimenters cited with the exception of Laneville and Parkinson (9) have verified the growth of the scale of the turbuelnce as the distance from the grid increased. Both methods used in this study for determination of the longitudinal integral length scales depend on the autocorrelation function so it is not surprising that they show similar trends in the variation of the scales. The estimates of the scales from the area under the autocorrelation curve are believed to be the most accurate because the autocorrelation function is used directly. The estimate of the scale from $G_x(0)$ indirectly involves the autocorrelation curve through the use of its Fourier transform. This transformation involves two approximations which reduce the accuracy of the estimates of the power spectrum at low frequencies. The theoretical power spectral density function as

calculated from the Fourier Transform of the autocorrelation curve is given by equation (6.2)

$$G_x(f) = 4\int_0^\infty R_x(\tau) \cos (2\pi f\tau)d\tau \quad . \tag{6.2}$$

First, a finite time autocorrelation function must be used. As a result, the low frequency information which is contained in the autocorrelation function for large values of τ is lost. Secondly, the Fourier transform of a finite length function automatically involves the transformation of an associated window function. If the true autocorrelation function, over the range for which values are known, is used then

$$\hat{G}_x(f) = 4\int_0^\infty R_x(\tau)\ \omega(\tau) \cos (2\pi f\tau)d\tau \tag{7}$$

where $\hat{G}_x(f)$ is an estimate of $G_x(f)$

and $\omega(\tau) = 1$ for $0 \leq \tau \leq T_m$ = the maximum delay

$$\omega(\tau) = 0 \text{ for } \tau > T_m \quad .$$

This is called the box car window function. Figure (8) shows that use of this window function produces estimates of the integral scale which are very close to those estimated from the area under the autocorrelation curve. Unfortunately, use of this type of window produces rough estimates of the power spectral density function as shown in Figure (11). Blackman and Tukey (11), Bendat and Piersol (12) and Enochson and Otnes (13) all present discussions of the effects of different shapes of lag windows on power spectral density estimates. Based on their discussions, a Hann lag window was used in estimating the power spectral density functions. The values of longitudinal

integral length scales represented by the closed data markers in Figure (7) were found from $G_x(0)$ using the Hann window function which is:

$$\omega(\tau) = 1/2(1 + \cos \frac{\pi t}{T_m}) \tag{8}$$

where

$$T_m = 0.05 \text{ seconds}$$

Use of the Hann Window Function results in estimates of the spectral density function at low frequencies which are smaller than the true density. This can be seen graphically in Figure (14). Figure (8) also includes some longitudinal integral length scales measured by Marshall (6), Bearman (10) and Laneville (9). The values of scale are of the same order of magnitude as those measured in this study. An interesting phenomena is hinted at by a comparison of the various data. Note that when Laneville (9) doubled his bar size and mesh size so that the (b/M) ratio was unchanged, the integral length scale did not increase proportionately. The (L_x/b) ratio actually decreased as the bar size increased. Marshall (6) and Bearman (10) used grids with approximately the same (b/M) ratio as the present study yet their (L_x/b) ratios are larger than those found at VPI & SU. In both cases as the number of meshes in the wind tunnel cross-section increased, the ratio of (L_x/b) increased. It seems probable that increasing the number of meshes increases the (L_x/b) ratio in a nonlinear fashion. When Laneville doubled his bar size and mesh size his grid contained one-fourth as many meshes as before. Both Bearman's and Marshall's

grids contained over ten times as many meshes as were contained in the grid used in this study. This indicates that there exists an optimum number of meshes, for a given tunnel size and bar width, which will produce the largest integral length scale.

Curves were fit through the values of the longitudinal integral length scales downstream of the grid for each of the three velocities. The form of the equation used to fit the data is based on the assumption that

$$\frac{dL_x}{dx} = C_1 \frac{\sqrt{\overline{u^2}}}{\overline{u}} \tag{9.1}$$

which Naudascher (14) indicates has proved successful in the analysis of flows past point and line sources of turbulent energy. Replacing the turbulence intensity with the empirical expression (4), the following is obtained.

$$\frac{dL_x}{dx} = 4.57\ C_1 b\left(\frac{1}{x}\right) \tag{9.2}$$

Separating variables and integrating produces:

$$L_x = 4.57\ C_1 b \ln x + C_2 \quad . \tag{9.3}$$

Now if C_2 is allowed to be a function of the velocity, the expression becomes:

$$L_x = 4.57\ C_1 b \ln x + [C_2' + C_2''\ \overline{u}\ ] \quad . \tag{9.4}$$

Solving for the constants by a least squares approach yields the following empirical relation.

$$L_x = .55\ b \ln X + .022\ \overline{u} - 5.46 \qquad (9.5)$$

C_1 was found to be 0.12. Figure (8) includes a plot of this curve for a mean velocity of 44.3 feet per second.

The lateral integral length scale was measured at four locations downstream of the grid. These scales were determined by using two hot wire anemometer probes. The correlation coefficient for zero time delay between the signals was determined for various lateral separations of the probes. The lateral integral length scale is defined as

$$L_y \equiv \int_0^\infty R(y)dy \quad . \qquad (2)$$

R(y) is assumed to approach zero for large displacements so the equation becomes in finite form

$$L_y = \int_0^{Y_m} R(y)dy \quad . \qquad (10)$$

The values of the lateral integral scales determined are shown in Figure (9). The values were found to be between 2 and 2.5 times smaller than the corresponding values of the longitudinal integral length scales as estimated from the empirical relation determined for the longitudinal scales of this study. Figure (10) compares the present results for lateral integral length scales with those found by Marshall (6) and Vickery (1). Agreement of results is also good when compared with the empirical formulation for lateral scale behind a grid with a (b/M) ratio of 0.2 as suggested by Dryden et al (2).

Power Spectral Density Estimates

Estimates for the power spectral density functions were obtained at the same nine positions behind the turbulence grid at which turbulence intensities and longitudinal integral length scales were measured. Figures (18 - 20) summarize the results of these estimates and indicate the major features. In the discussion of integral length scales the variation in power spectral densities due to the use of different window functions was mentioned. Figure (11) shows how the estimates of the spectral density function for the same autocorrelation function are affected by using a Box Car window or Hann windows with two different maximum time delays. The use of these window functions is further illustrated in Figures (12 - 15).

The estimate of the power spectral density function was expressed in equation (7). Using the two sided form of the power spectral density function, the equation becomes

$$\hat{S}_X(f) = \int_{-\infty}^{\infty} \omega(\tau) R_X(\tau) \cos(2\pi f\tau) d\tau \quad . \tag{7}$$

Now if W(f) is the Fourier transform of $\omega(\tau)$.

$$W(f) = \int_{-\infty}^{\infty} \omega(\tau)\, e^{-i2\pi f\tau}\, d\tau \quad . \tag{11}$$

Then another expression for the estimate of the power spectral density function is given by references (11), (12), and (13) to be:

$$\hat{S}_X(f) = \int_{-\infty}^{\infty} S_X(n) W(f - n) dn \quad . \tag{12}$$

Where $S_x(n)$ is the true spectrum and equal to one half the one sided true spectrum. Equation (12) shows that, if the true power spectral density function is known and if the Fourier transform of the lag window function is determined, then the effects of using a particular lag window can be measured. Figure (12) shows the Fourier transform of the Hann window, equation (8), for the two values of the maximum delay or lag time, T_m, used in analysis of data for this study. Figure (13) shows the Fourier transform of the Box Car window with $T_m = 0.05$ sec. The physical interpretation of the convolution in equation (12) is to shift the center frequency of the window function transform from zero to f, multiply values of the true spectrum by this shifted window function and then to integrate over the frequency range. The resulting estimate of the power spectrum represents an average of the true power spectrum for frequencies around f. In 1948 von Karman (15) proposed an emperical formula of the form

$$F(K_1/K_0) = \text{const.} \frac{1}{[1 + (K_1/K_0)^2]^{5/6}} \tag{13}$$

to represent the one dimensional power spectral density function of the longitudinal velocity component in isotropic turbulence. The expression is designed to represent the spectrum of the energy containing eddies down to the inertial subrange. This equation has been slightly modified and used to represent atmospheric turbulence. The presently accepted form of the von Karman spectrum equation for the longitudinal turbulence component as listed by Teunissen (16), Gault and Gunter (17) and Templin (18) is;

$$\Phi(n) = \frac{4\,\dfrac{L_x}{\bar{u}}}{\left[1.0 + \text{const.}\left(\dfrac{nL_x}{\bar{u}}\right)^2\right]^{5/6}} \tag{14}$$

where const. = 70.78 .

If this equation is used as the true spectrum in equation (12), an estimate of the spectrum can be determined for the three windows whose transforms are shown in Figures (12) and (13). The estimates of the von Karman spectrum, for the three lag windows, are compared with the original von Karman spectrum in Figures (14) and (15). Figure (14) shows that use of the Hann lag window produces estimates of the power spectral density which are lower than the true spectrum for values of $(nL_x/\bar{u})$ less than 0.1 and accurate estimates if $(nL_x/\bar{u})$ is greater than 0.3 provided the spectrum is of the shape of the von Karman spectrum. Use of the Box Car window produces better estimates of the power spectrum at values of $(nL_x/\bar{u})$ less than 0.05 than those produced by use of the Hann window. However, use of the Box Car window produces some unexpected deviations in the estimates for values of $(nL_x/\bar{u})$ greater than about 0.07, Figure (11). Based on the results of Figure (11) along with the comparison of estimates in Figures (14) and (15) the Hann lag window was used in calculating the power spectral density estimates from autocorrelation functions of data taken in this study. Furthermore, the autocorrelation function with a maximum delay time of 0.05 sec. was used because of the analysis time involved. Twice as much analysis time was required to create an autocorrelation function with T_m = 0.10 sec. as was required to create an autocorrelation function

with T_m = 0.05 sec. Figure (14) shows that deviations of the estimated spectrum from the true spectrum, due to the finite maximum delay time, are regular and can be predicted for a smooth spectrum function like the von Karman Spectrum Function. Figure (16) compares the von Karman Spectrum Function with four experimentally determined spectrum estimates for the flow behind the grid. These experimentally determined spectra are very close in both shape and magnitude to the von Karman Spectrum Function. Furthermore, the Hann window with a maximum delay time of 0.05 sec. was used in determining the experimental estimates. It can be seen from Figure (16) that the experimental estimates deviate from the von Karman equation in much the same way that the empirical estimate for T_m = 0.05 sec. in Figure (14) deviates from the von Karman equation. Therefore, an attempt was made to remove the effects of a particular maximum delay time. For any given frequency, both the value of the von Karman equation and the estimate of the von Karman equation from equation (12) could be determined. Subtracting the value of the estimate from the true value and dividing by the value of the estimate gives the factor which can be used to obtain the true value from the estimate. Since the shape of the experimentally determined estimate was similar to the shape of the empirically determined estimate from equation (12), the correction factors were used to improve the values of the experimentally determined spectral density estimates. Figure (17) shows improved estimates for the experimentally determined spectra in Figure (11) which were calculated using the Hann window with T_m = 0.05 sec. and T_m = 0.10 sec. The two improved estimates agree well with each other and with the von Karman equation. This indicates that the effect of the

length of the autocorrelation curve used in obtaining spectral density estimates can be reduced significantly. Since the estimates are very similar, either autocorrelation function can be used and the use of the shorter maximum time delay is justified. An additional advantage of using the maximum time dealy of 0.05 sec. as opposed to 0.10 sec. is that the estimated spectral density functions are smoother. The reason the estimate is smoother can be deduced from equation (12) and Figure (12). The smaller value of T_m causes the Fourier transform of the Hann window, W(f), to have a broader central lobe than W(f) for the larger T_m. Consequently, when the convolution in equation (12) is performed, the estimate of the power spectral density is the average of the spectral density for a broader band of frequencies around f for W(f) with T_m = 0.05 sec. than the estimate with T_m = 0.10 sec.

Figures (18) through (20) present improved spectral density estimates at four locations downstream of the grid and for three different values of the mean velocity. The estimated spectral densities seem to be independent of velocity and distance downstream of the grid. The shape of the spectral density curves are in close agreement with the von Karman equation as presently accepted for atmospheric turbulence but the values of the spectral density measured in the wind tunnel are a little higher than those predicted by the von Karman equation for $(nL_x/\bar{u})$ greater than 0.07. If the constant used in the von Karman equation is reduced from 70.78 to approximately 64.0, the agreement between the experimental and empirical estimates is greatly improved. Figure (21) shows the changes in the von Karman spectral density estimates resulting from use of a smaller value of the constant.

The improved estimates of the experimentally determined power spectral density functions are based on the von Karman equation with the constant equal to 70.78 instead of 64.0. However, use of the von Karman equation with the constant equal to 64.0 in determining the improved experimental estimates would only cause second order changes in the estimates from those presented in Figures (18) through (20). The von Karman equation with the constant equal to 70.78 is fairly close in both magnitude and shape to the improved spectral density estimates.

The basis for the use of 70.78 as the constant in the generally accepted form of the von Karman equation is unclear. The origin of this value was never stated in references (16), (17), and (18). The value can be determined; however, if the Harris' spectrum equation (19) is used as a starting point. Harris modified Davenport's (20) expression for the spectrum of the longitudinal velocity component of atmospheric turbulence and proposed that

$$\frac{n\,G(n)}{\overline{V}_{10}^{\,2}} = \frac{4\,K\,\tilde{n}}{(2 + \tilde{n}^2)^{5/6}} \tag{15}$$

where:

$n = n\cdot(1800 \text{ metres}) \,/\, \overline{V}_{10}$

K = a surface drag coefficient

$\overline{V}_{10}$ = the mean velocity at a height of 10 meters .

Transforming this equation to the nondimensional form used in this report can be accomplished by using several approximate empirical expressions for atmospheric flow characteristics developed by Harris (19)

and Davenport (20).

$$\frac{\sqrt{\overline{u^2}}}{\overline{u}_z} = 2.58\ K^{1/2}\ (\frac{10}{z})^a \tag{16}$$

where (a) is the power law exponent of the velocity profile and (z) refers to the height above ground. ($\overline{u}_z$) refers to the mean velocity at a height z instead of the mean velocity in the z direction.

Also:

$$L_x = 151(\frac{z}{10})^a \text{ metres} \tag{17}$$

and

$$\overline{u}_z = \overline{V}_{10}(\frac{z}{10})^a \quad . \tag{18}$$

Use of these three expressions in equation (15) transforms it to,

$$\frac{n\ G(n)}{\overline{u^2}} \doteq \frac{4\ \dfrac{nL_x}{\overline{u}}}{\left[1.0 + 71.05\left(\dfrac{nL_x}{\overline{u}}\right)^2\right]^{5/6}} \tag{19}$$

which is the von Karman equation for atmospheric turbulence with a slightly altered constant. It should be noted that this form of the equation is consistent with the theoretical predictions that:

1) $L_x = \dfrac{G(0)\overline{u}}{4\ \overline{u^2}}$

2) The slope of the power spectrum equation for large values of ($nL_x/\overline{u}$) follows a negative 5/3 power law.

These conditions are satisfied regardless of the value of the constant. Comparison of the equation with experimental measurements of longitudinal wind spectra in Harris (19) Davenport (20) and Templin (18) indicates that there is enough variation in measured spectra to support the use of a lower value of the constant to represent atmospheric turbulence.

Use of the Flow in Model Tests

The turbulent flow produced by a uniform grid can be used in sectional model studies of suspension bridges to simulate the atmospheric flow conditions. The atmospheric flow will be simulated exactly if the ratio of integral length scales for the prototype and model conditions is equal to the ratio of the prototype dimensions to the model dimensions.

$$\frac{L_{x_p}}{L_{x_m}} = \frac{D_p}{D_m}$$

The integral length scales currently produced in the wind tunnel are too small to allow geometric scaling to be satisfied and to allow use of reasonably sized models. There are some indications that geometric scaling of the integral length scales is not critical to model response. Laneville and Parkinson (9) state that no appreciable effect of scale size was found in the galloping of rectangular cylinders for integral length scales of the same order of magnitude as the model dimensions. Measurements were made of the galloping of a square cylinder for ratios

of (L_x/D) varying from 1.58 to 5.0. No appreciable change in response was noted. Bearman (10) shows that the ratio (L_x/D) does have an effect on the fluctuating drag forces on a flat plate at low frequencies. He shows that for values of $(nD/\bar{u})$ greater than 0.2, the power spectral density estimates of the fluctuating drag are invariant for (L_x/D) greater than 0.5. This would tend to indicate that as long as the range of frequencies of interest in a bridge model study is high, the effects of using improper integral length scales will be negligible. More work using various (L_x/D) ratios will have to be performed before the requirements for scales can be adequately resolved.

CONCLUSIONS

The turbulent flow field generated in the VPI & SU wind tunnel by an obstruction in the from of a coarse grid is analyzed to have properties similar to those measured behind other grids. A notable exception is that the longitudinal integral length scale was found to be velocity dependent. The reason this phenomena has not been measured previously is probably due to equipment deficiencies and the fact that most previous studies primarily included measurements of the lateral integral length scale. The lateral integral length scale is less than half as large as the longitudinal integral length scale so scale changes due to velocity variations would be much smaller and consequently could be hidden by the experimental scatter. It should be noted that many previous studies show four or five times greater scatter of data than does the present study. Newer equipment and shorter length hot wires has increased the accuracy of recent measurements. The papers published since 1965 show much better agreement on turbulence intensity measurements than do papers published before that date.

An investigation was conducted to determine the effects of using finite length autocorrelation functions in determining power spectral density estimates. Results show that the use of a particular length autocorrelation function causes specific deviations in the power spectral density estimates which are calculated. It was concluded that for a smooth power spectrum function the deviations are regular and can be predicted if the functional form of the true spectrum is known.

Corrections can then be made which compensate for the deviations and produce improved power spectral density estimates. When two autocorrelation functions, for the same turbulence signal, involving two different maximum time delays were used, and their corresponding improved spectral density estimates were determined, the resulting spectra agreed very well. Their corresponding unimproved estimates displayed relatively large differences in spectral density values especially for energy in low wave number eddies. The effects of using a finite length autocorrelation curve in determing spectral density estimates can be reduced by the use of a data window with properties like the Hann window. The estimates can be further improved by correcting deviations caused by use of the window function if the form of the true spectral density function is known.

Experimentally determined power spectral density estimates for the longitudinal turbulence component were found to agree very well with full scale power spectral density estimates. The von Karman one dimensional spectrum equation was found to be an accurate empirical expression for the spectrum of the longitudinal component of grid turbulence. The value of the constant in the von Karman equation for a good fit to the spectra of grid turbulence was found to be approximately 64.0 while several authors pick a constant of 70.78 for a good fit to full scale atmospheric spectral data. Scatter in full scale spectral data indicates that use of 64.0 as the constant in the von Karman equation also produces an expression which is representative of atmospheric spectra.

Grid induced turbulent flow can be used to simulate atmospheric flow conditions in sectional model studies of suspension bridges and other

elevated structures. The flow conditions will be simulated exactly if geometric scaling of structural dimensions and integral length scales is satisfied. Results by other investigators indicate that for integral length scales of the order of magnitude of the model dimensions and larger, the dynamic forces are not dependent on the integral length scale. Thus with some caution, the use of models of the same size as the integral length scale is justified.

REFERENCES

1. Vickery, B. J., "On the Flow Behind a Coarse Grid and its Use as a Model of Atmospheric Turbulence in Studies Related to Wind Loads on Buildings," NPL Aero Report 1143, March 1965.

2. Dryden, Hugh L., Schubauer, G. B., Mock, W. C., Jr., and Skramstad, H. K., "Measurements of Intensity and Scale of Wind-Tunnel Turbulence and their Relation to the Critical Reynolds Number of Spheres," NACA TR No. 581, 1937.

3. Baines, W. D., and Peterson, E. G., "An Investigation of Flow Through Screens," Transactions of the ASME, 73, July 1951, pp. 467-477.

4. Taylor, G. I., "Statistical Theory of Turbulence, Parts I-IV," (from "Proceedings of the Royal Society," A 151, 421-478 [1935]), Friedlander, S. K. and Topper, Leonard, Turbulence, Classical Papers on Statistical Theory, Interscience Publishers, Inc., New York, 1961, pp. 18-76.

5. Von Karman, T., and Howarth, L., "On the Statistical Theory of Isotropic Turbulence," (from "Proceedings of the Royal Society," A 164, 192-219 [1938], Friedlander, S. K., and Topper, Leonard, Turbulence, Classical Papers on Statistical Theory, Interscience Publishers, Inc., New York, 1961, pp. 76-99.

6. Marshall, Richard D., "Pressure Fluctuation Correlations Near an Axisymmetric Stagnation Point," Ph.D. dissertation, Colorado State University, Fort Collins, Colorado, June 1968.

7. Stewart, R. W., and Townsend, A. A., "Similarity and Self-Preservation in Isotropic Turbulence," Phil. Trans. Roy. Soc. London, 243A, June 1951, pp. 359-386.

8. Walshe, D. E. J., Wind-Excited Oscillations of Structures, National Physical Laboratory, Her Majesty's Stationery Office, London, 1972.

9. Laneville, A., and Parkinson, G. V., "Effects of Turbulence on Galloping of Bluff Cylinders," Proceedings of the Third International Conference on Wind Effects on Buildings and Structures, Tokyo, 1971.

10. Bearman, P. W., "An Investigation of the Forces on Flat Plates Normal to a Turbulent Flow," Journal of Fluid Mechanics, Vol. 46, Part I, 1971, pp. 177-198.

11. Blackman, R. B. and Tukey, J. W., The Measurement of Power Spectra, Dover Publications, Inc., New York, 1958.

12. Bendat, J. S., and Piersol, A. G., Random Data: Analysis and Measurement Procedures, Wiley-Interscience, New York, 1971.

13. Enochson, Loren D., and Otnes, Robert K., Programming and Analysis for Digital Time Series Data, Naval Publication and Printing Service Office, Washington, D. C., 1968.

14. Naudascher, Eduard, and Farell, Cesar, "Unified Analysis of Grid Turbulence," Journal of the Engineering Mechanics Division, Proceedings of the ASCE, April 1970, pp. 121-141.

15. Von Karman, Th., "Progress in the Statistical Theory of Turbulence," Proc. Nat. Acad. Sci. U. S., 34, 1948, p. 530.

16. Teunissen, H. W., "Characteristics of the Mean Wind and Turbulence in the Planetary Boundary Layer," UTIAS Review No. 32, October 1970.

17. Gault, J. D., and Gunter, D. E., Jr., "Atmospheric Turbulence Considerations for Future Aircraft Designed to Operate at Low Altitudes," AIAA Paper No. 68-216, Presented to the AIAA Aircraft Design for 1980 Operations Meeting, Washington, D. C., February 12-14, 1968.

18. Templin, R. J., "Interim Progress Note on Simulation of Earth's Surface Winds by Artifically Thickened Wind Tunnel Boundary Layers," National Aeronautical Establishment of Canada, Low Speed Aerodynamics Section Report LTR-LA-22, February 1969.

19. Harris, R. I., "The Nature of the Wind," Discussion, Proc. Construction Industry Research and Information Association, Seminar on the Modern Design of Wind-Sensitive Structures, C.I.R.I.A., London, 1971.

20. Davenport, A. G., "The Spectrum of Horizontal Gustiness Near the Ground in High Winds," Q.J. Roy. Met. Soc., Vol. 87, April 1961, pp. 194-211.

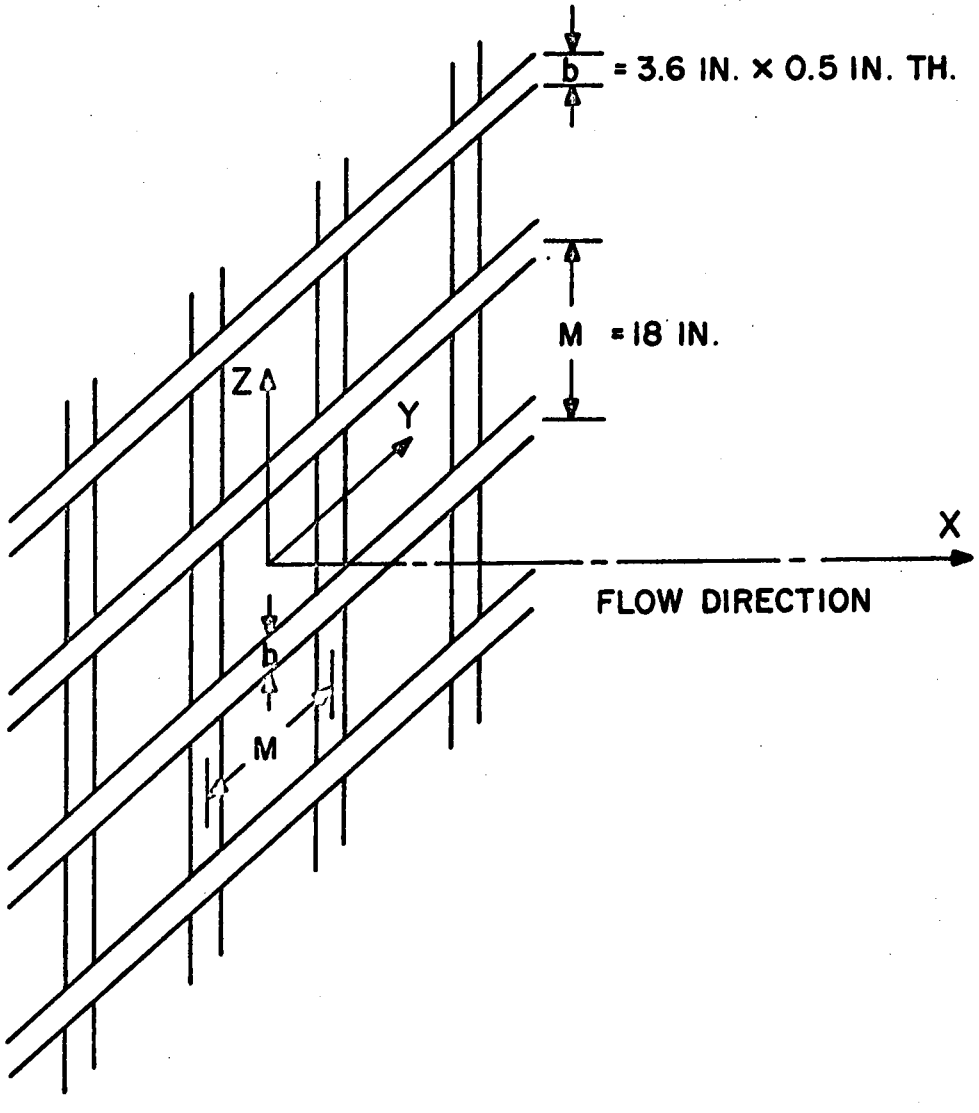

Figure 1: Grid arrangement and definition of axes sketch.

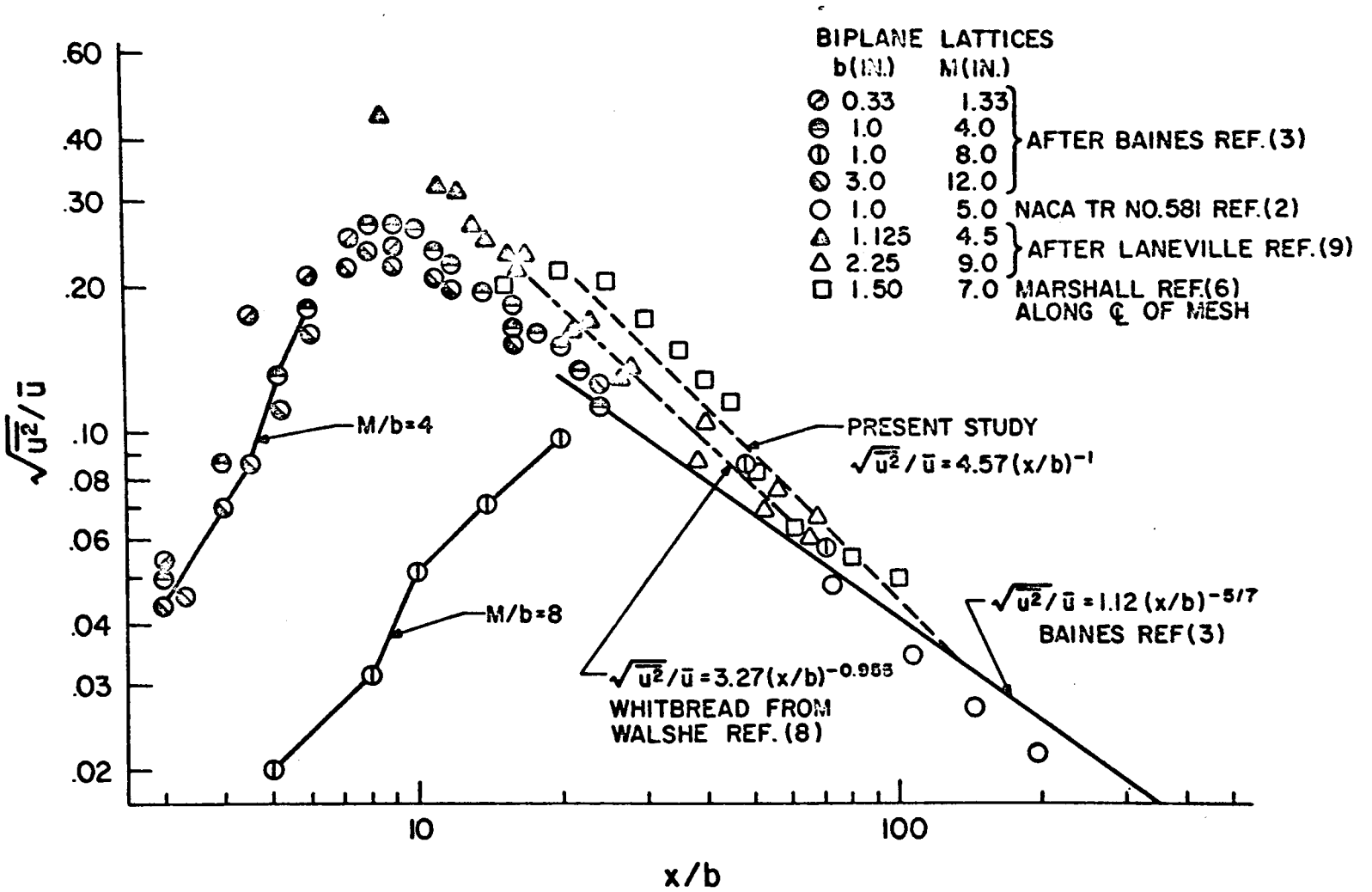

Figure 2: Comparison of turbulence intensity variations downstream of a grid.

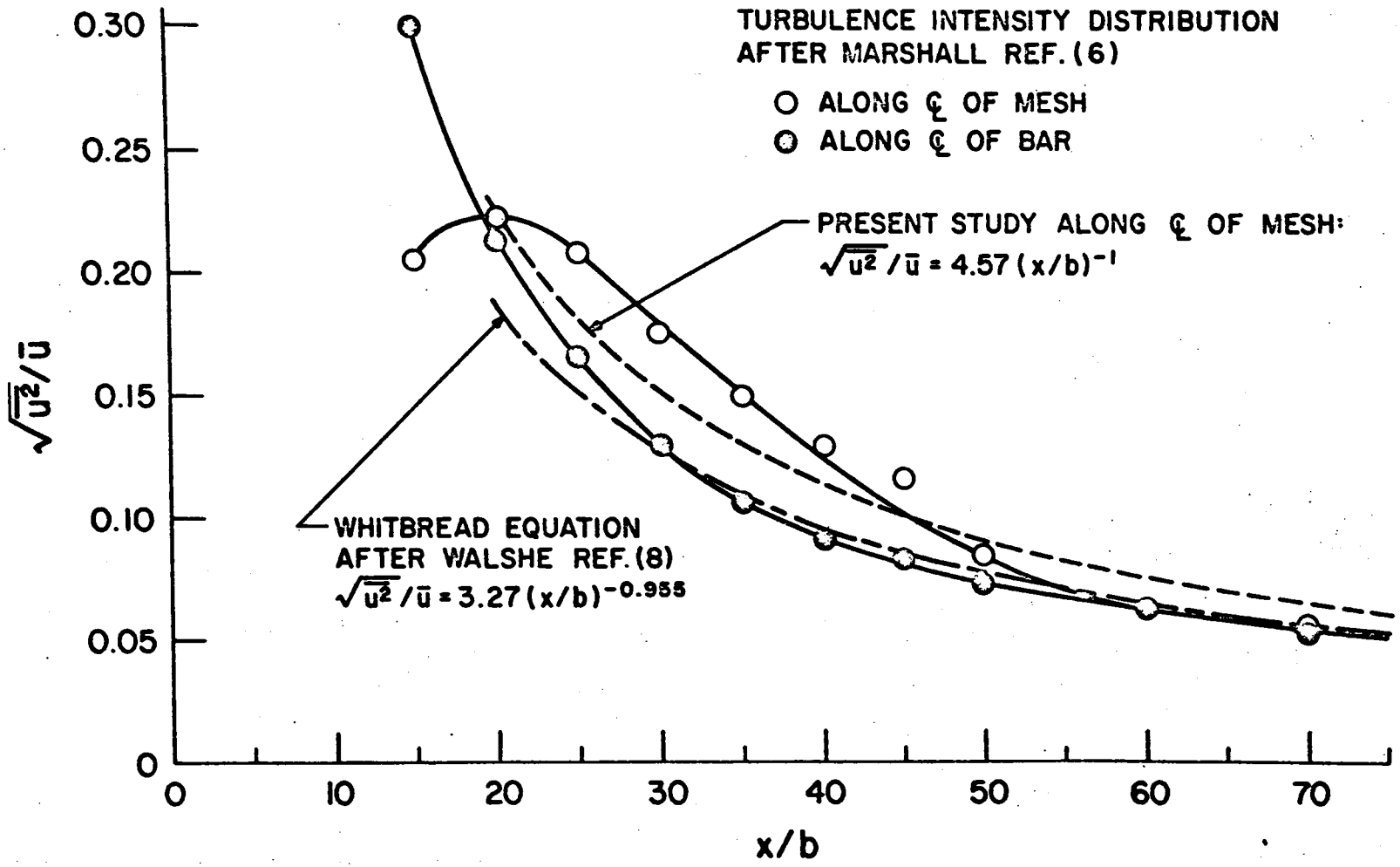

Figure 3: Variation of turbulence intensity behind mesh and bar.

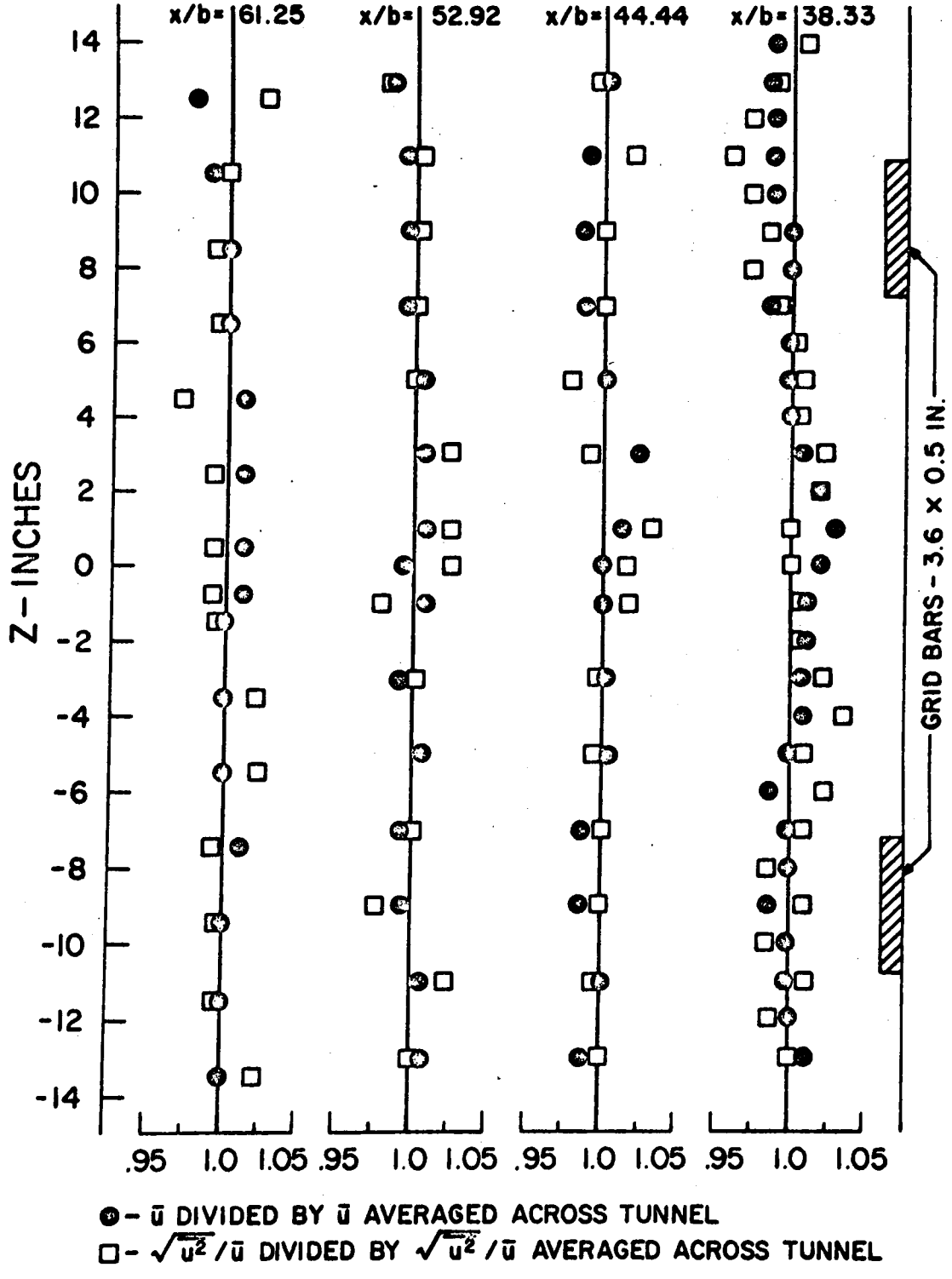

Figure 4: Variation of mean velocity and turbulence intensity across tunnel.

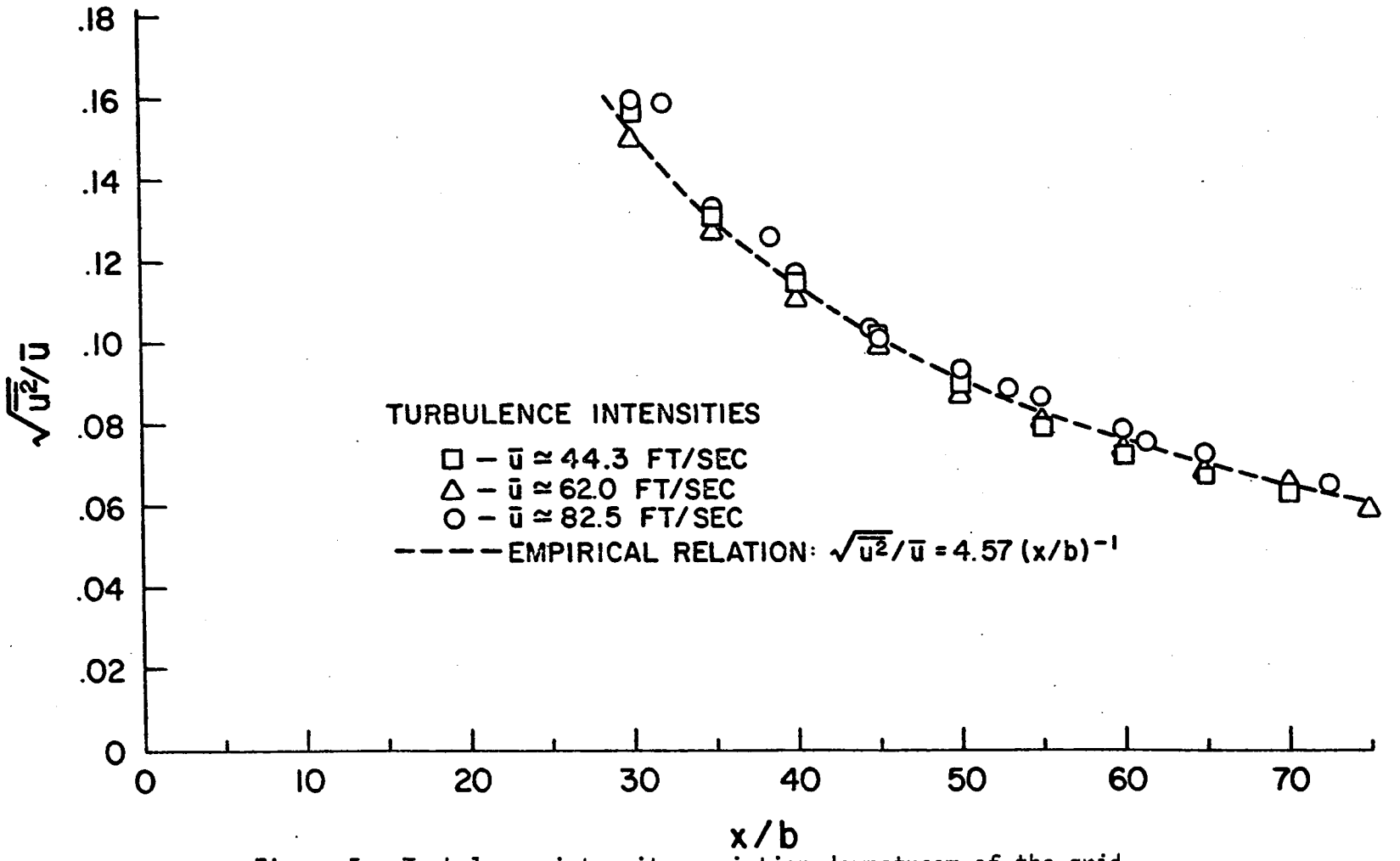

Figure 5: Turbulence intensity variation downstream of the grid.

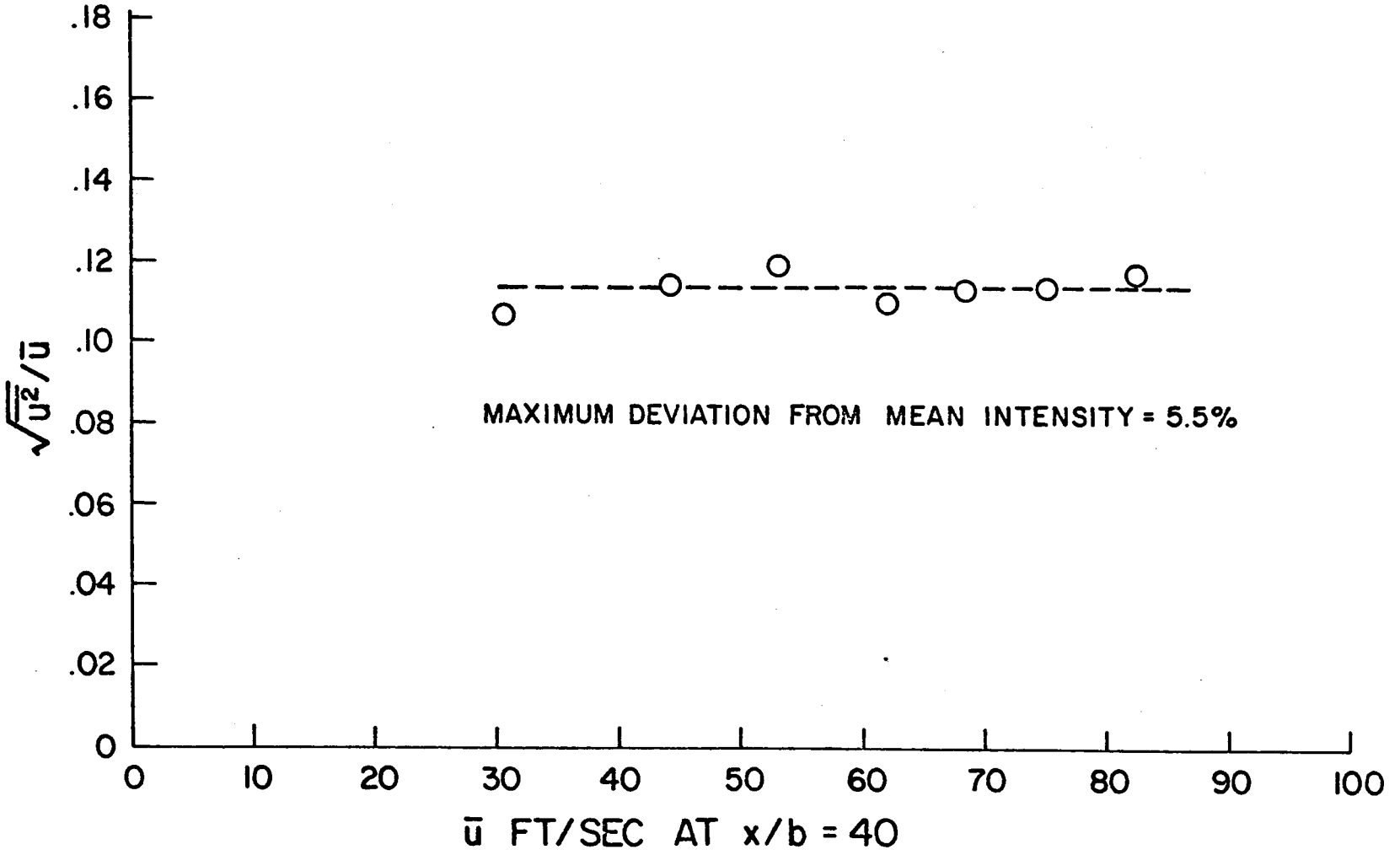

Figure 6: Turbulence intensity variation with velocity.

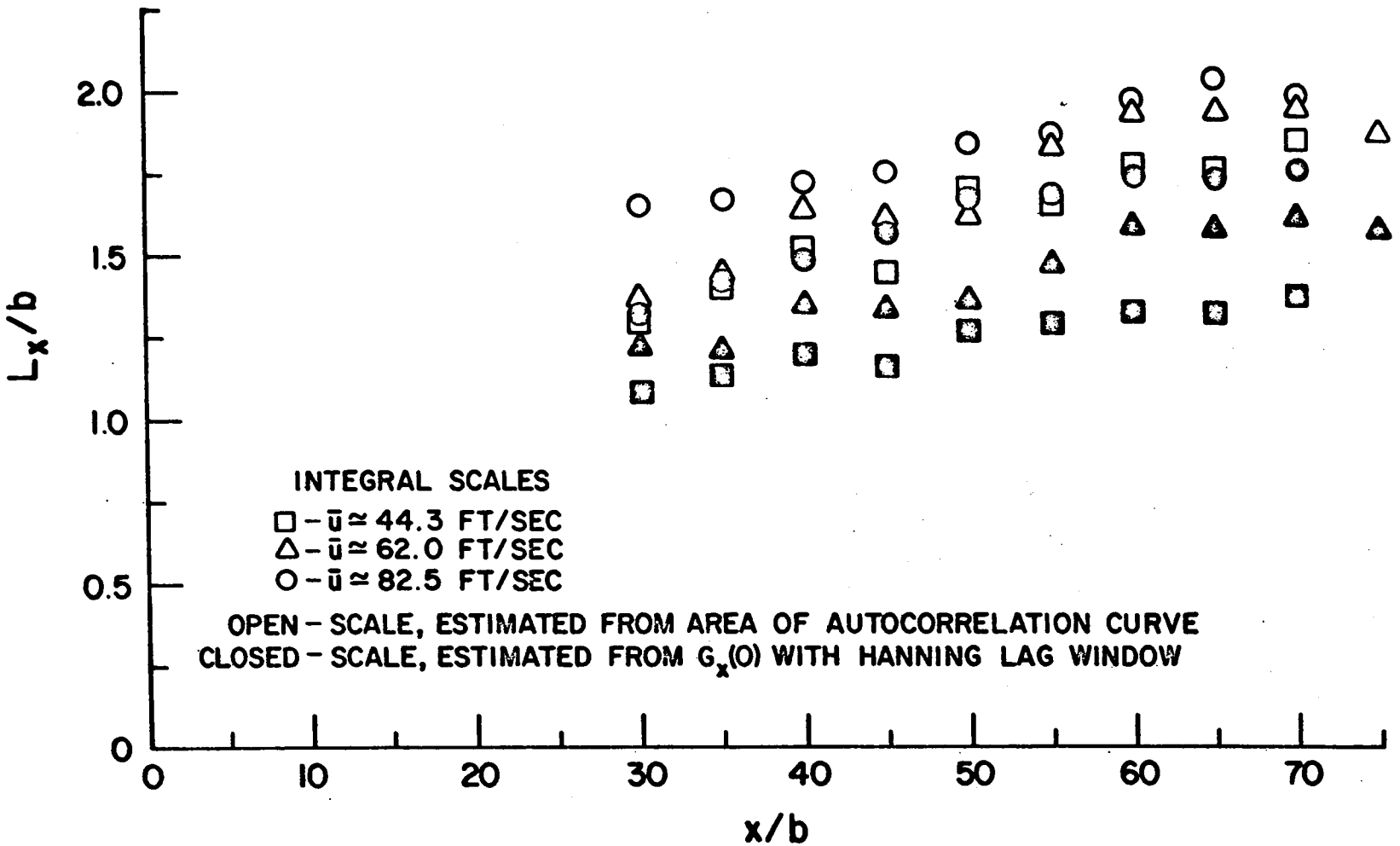

Figure 7: Variation of longitudinal integral length scale behind the grid.

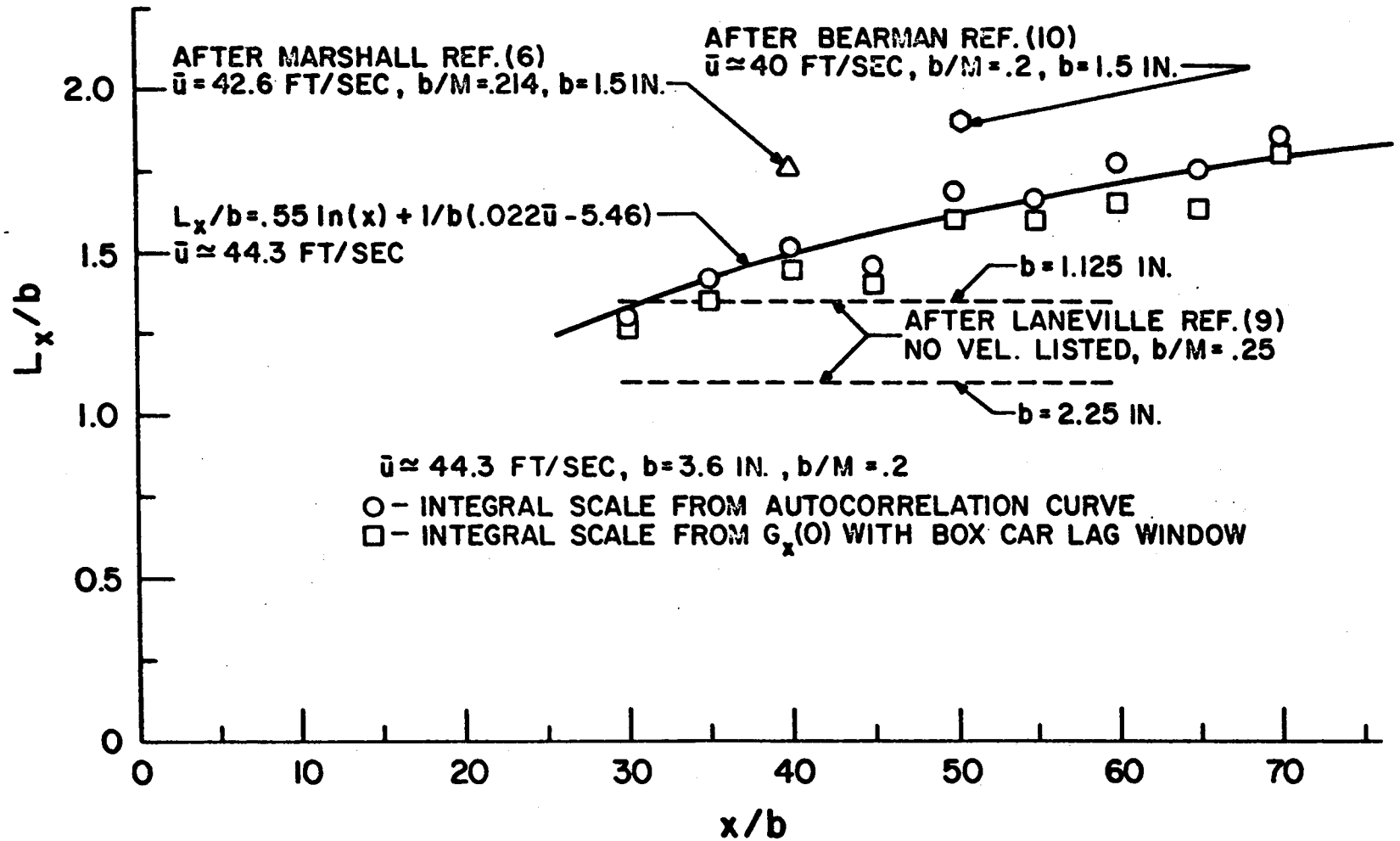

Figure 8: Comparison of longitudinal integral length scales behind grids.

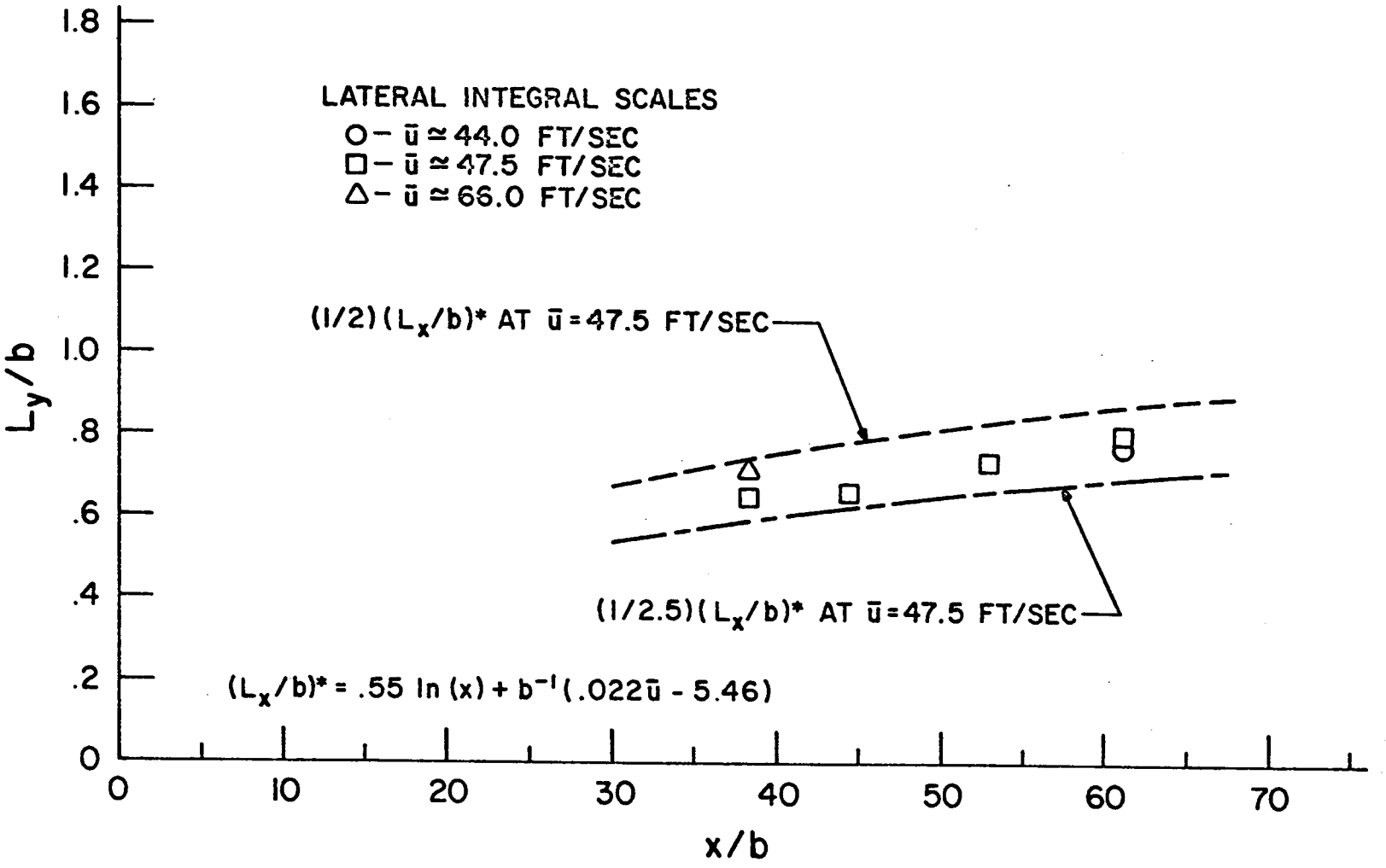

Figure 9: Variation of lateral integral length scale behind the grid.

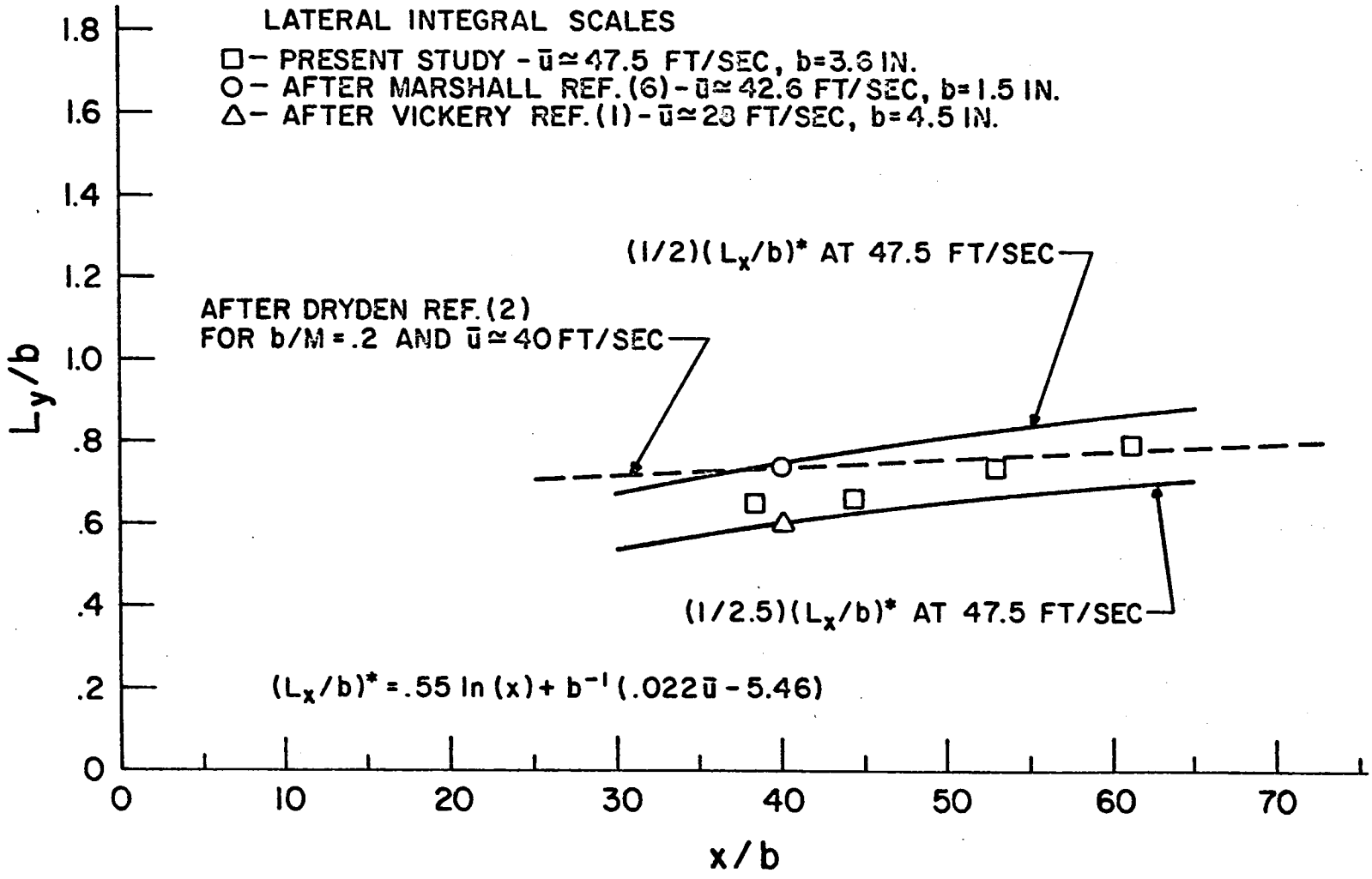

Figure 10: Comparison of lateral integral length scales behind grids.

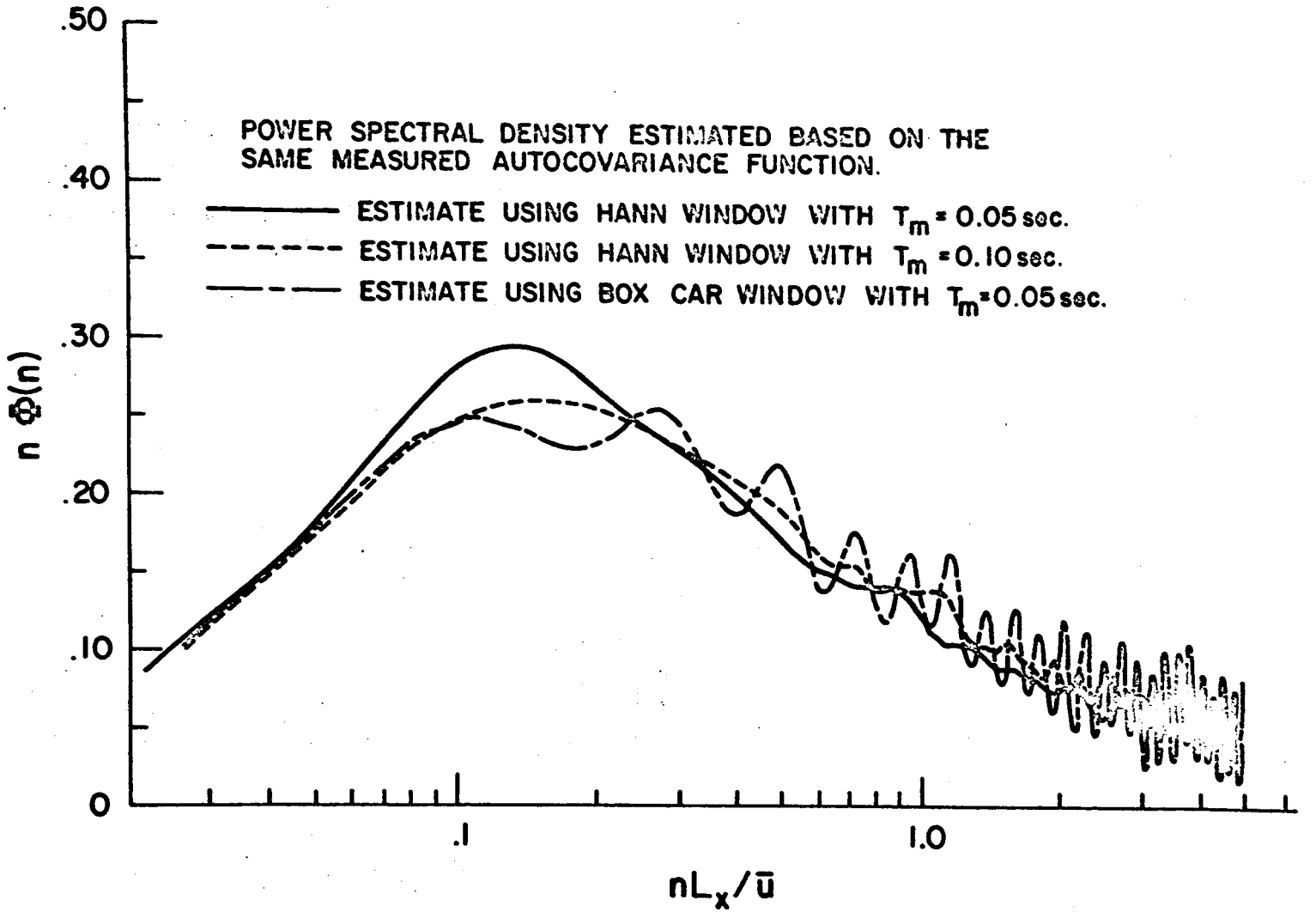

Figure 11: Estimates of the power spectral density function for X/b = 50 and $\bar{u}$ = 43.5 ft./sec. based on three different window functions.

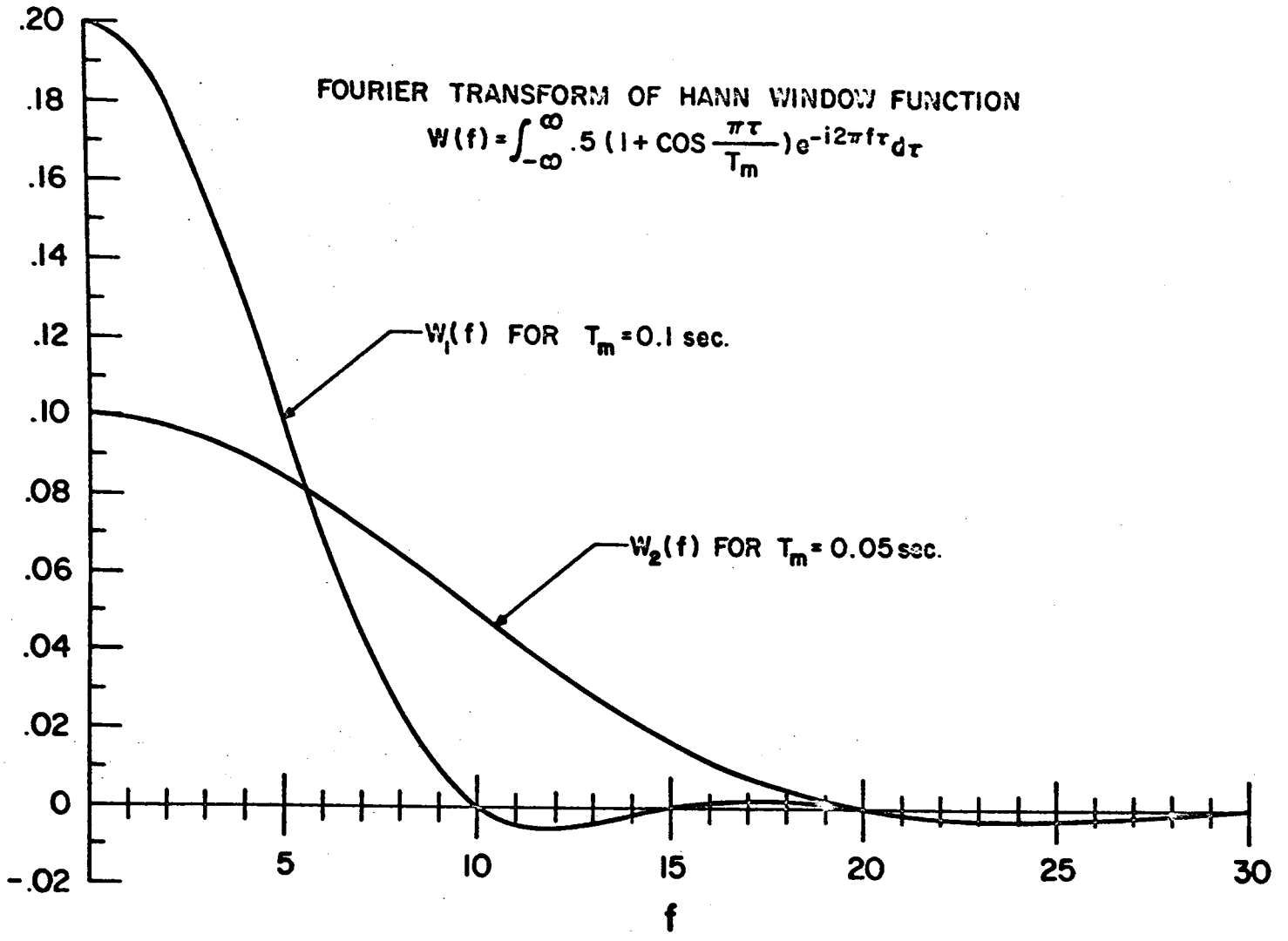

Figure 12: Fourier transforms for Hann windows of two max. time delays.

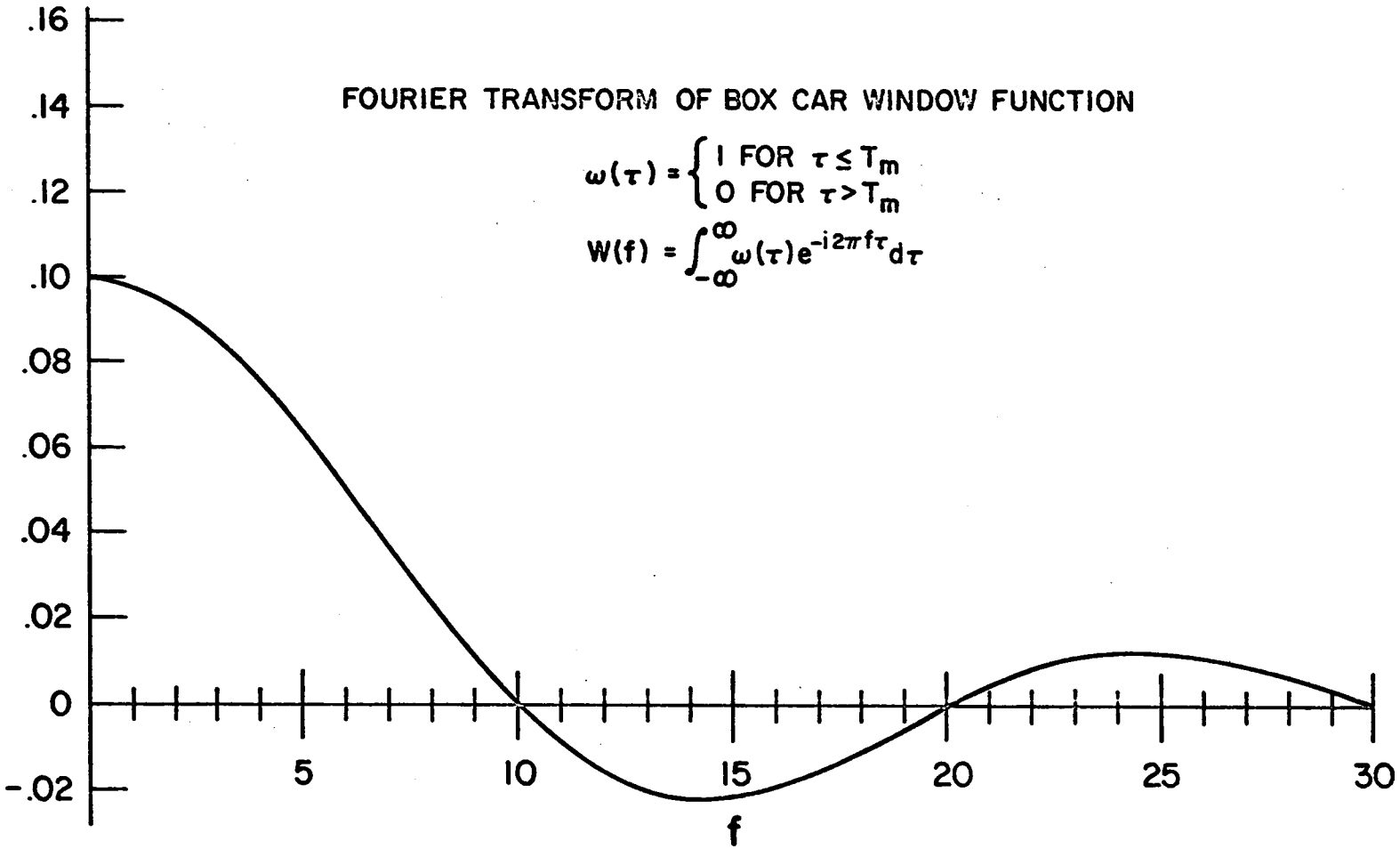

Figure 13: Fourier transform of Box Car window function with T_m = 0.05 sec.

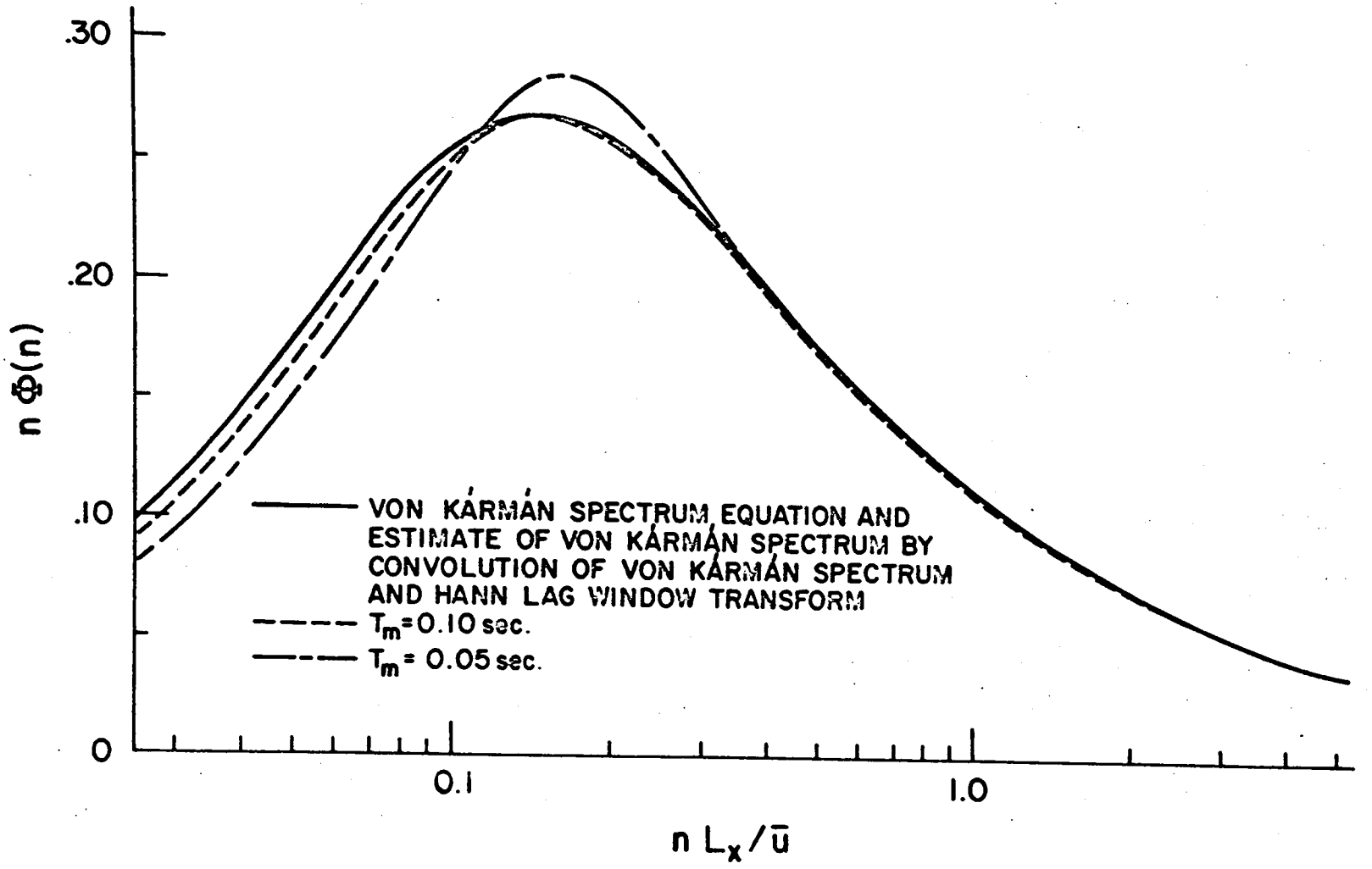

Figure 14: Comparison of estimates of von Karman spectrum, based on Hann lag windows of two lengths, with the true von Karman spectrum.

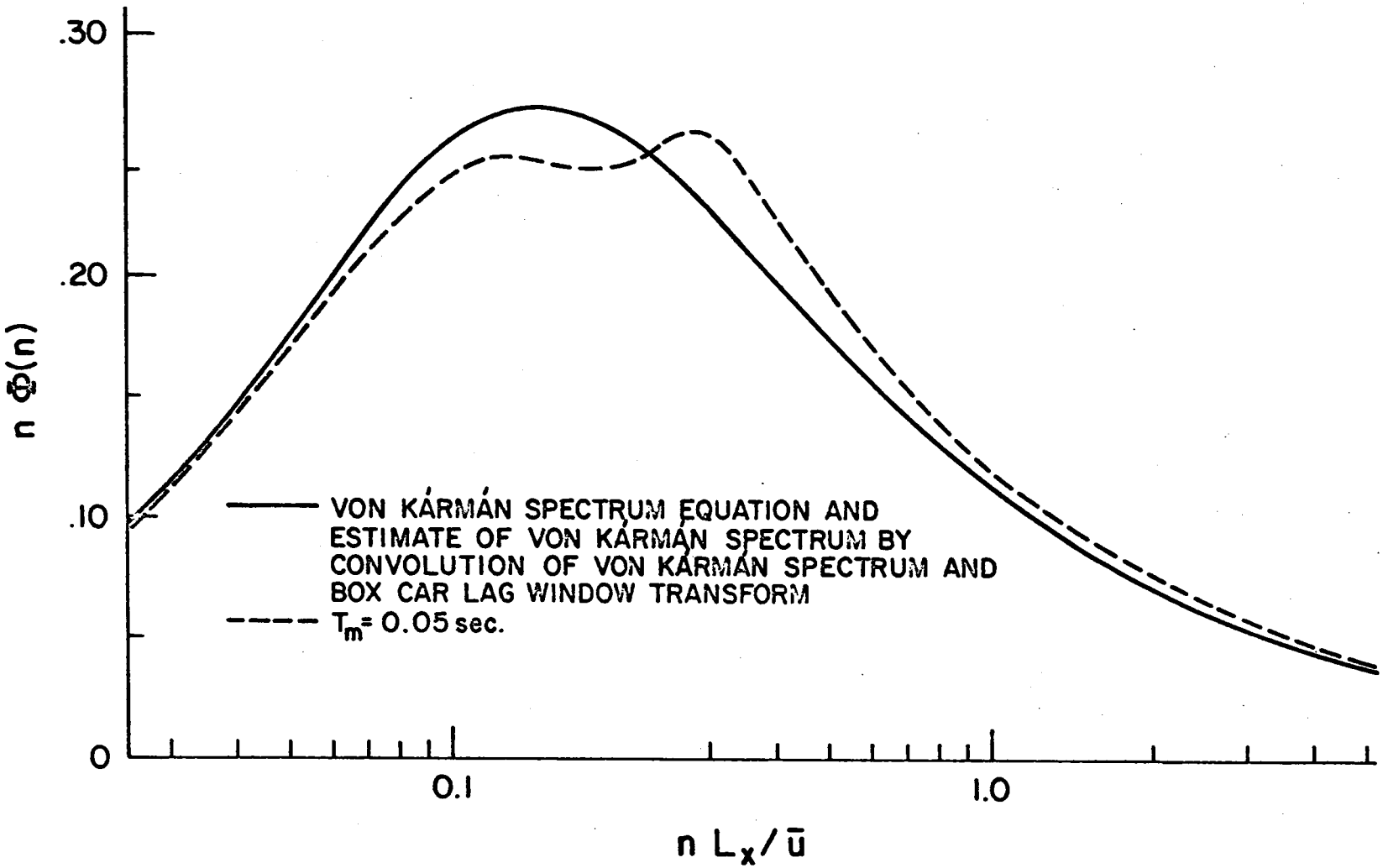

Figure 15: Comparison of an estimate of the von Karman spectrum, based on a Box Car lag window, with the true von Karman spectrum.

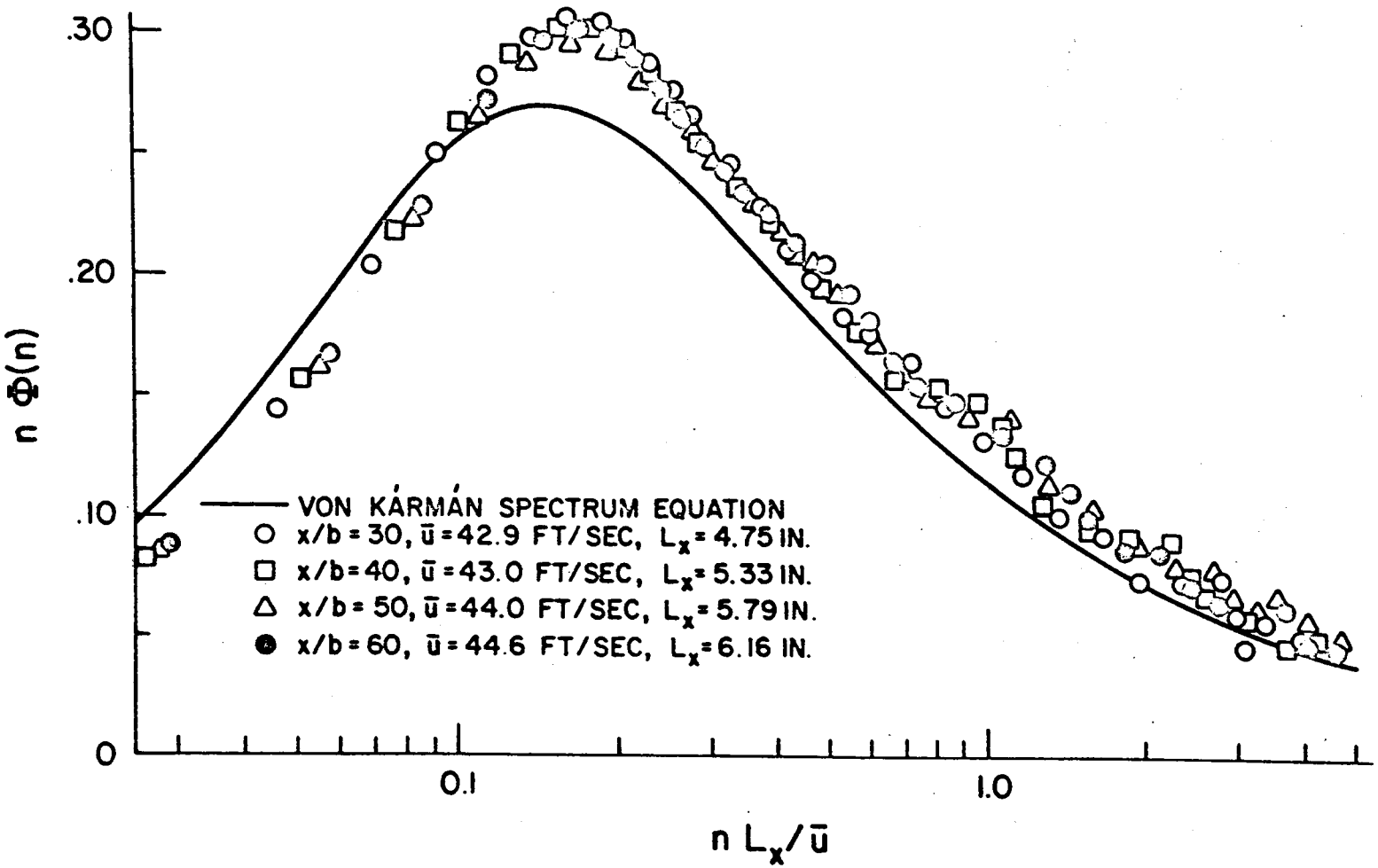

Figure 16: Normalized spectrum behind grid for $\bar{u} \approx 43.5$ ft./sec. using Hann window with $T_m = 0.05$ sec.

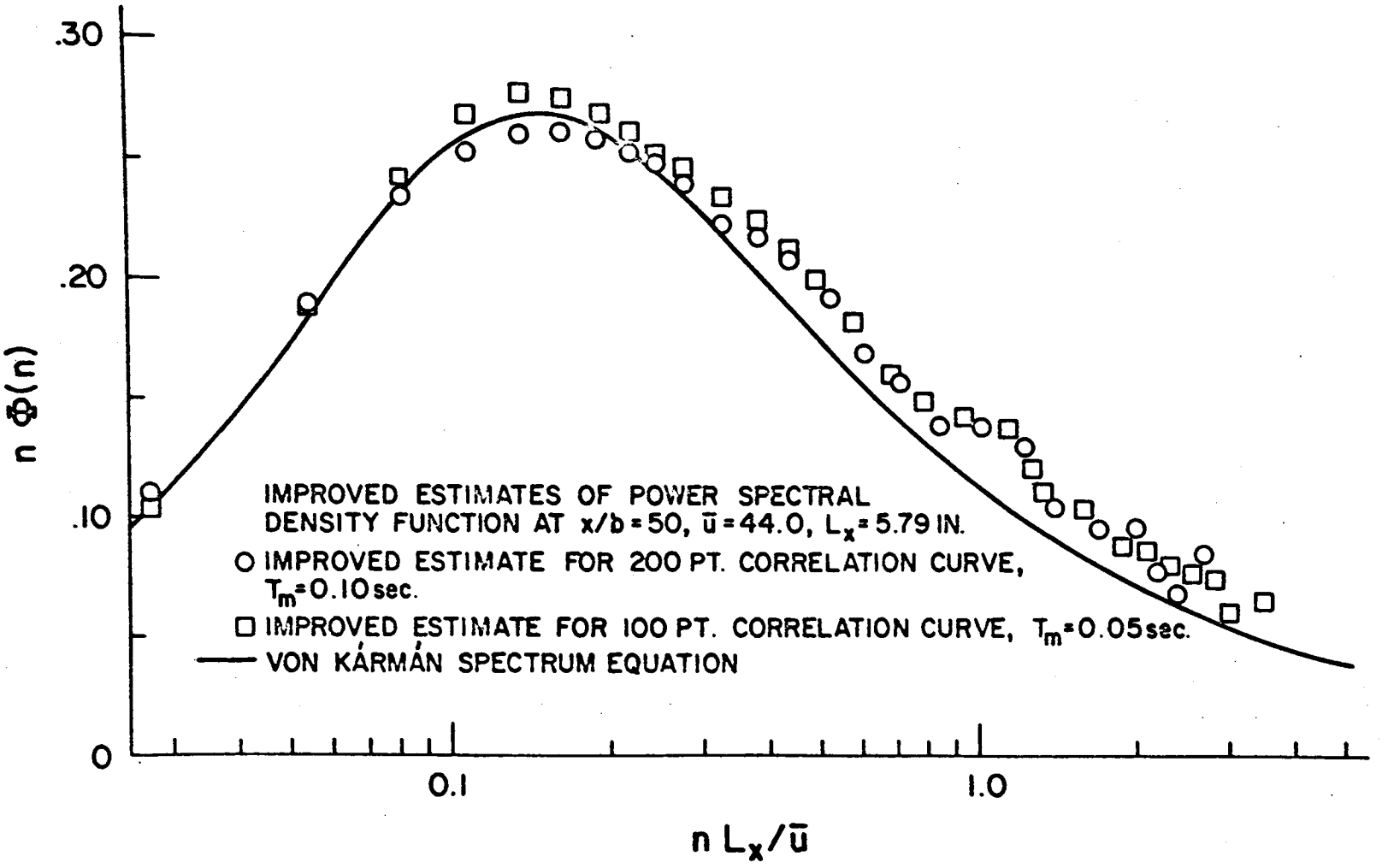

Figure 17: Improved estimates of power spectral density function shown in Figure 11 for the two Hann windows using corrections developed from information in Figure 14.

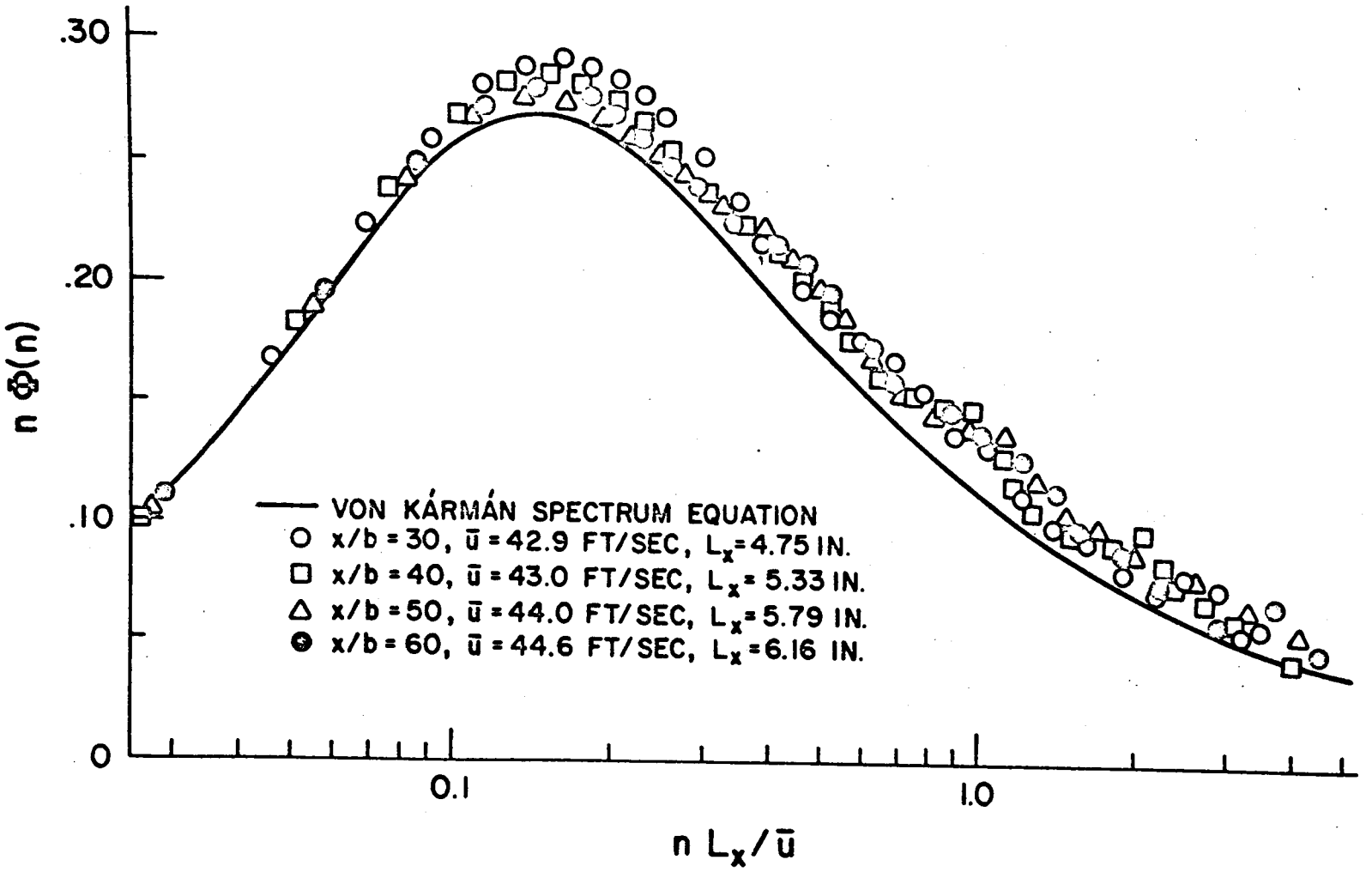

Figure 18: Improved estimates of power spectral density behind grid for $\bar{u} \approx 43.5$ ft./sec.

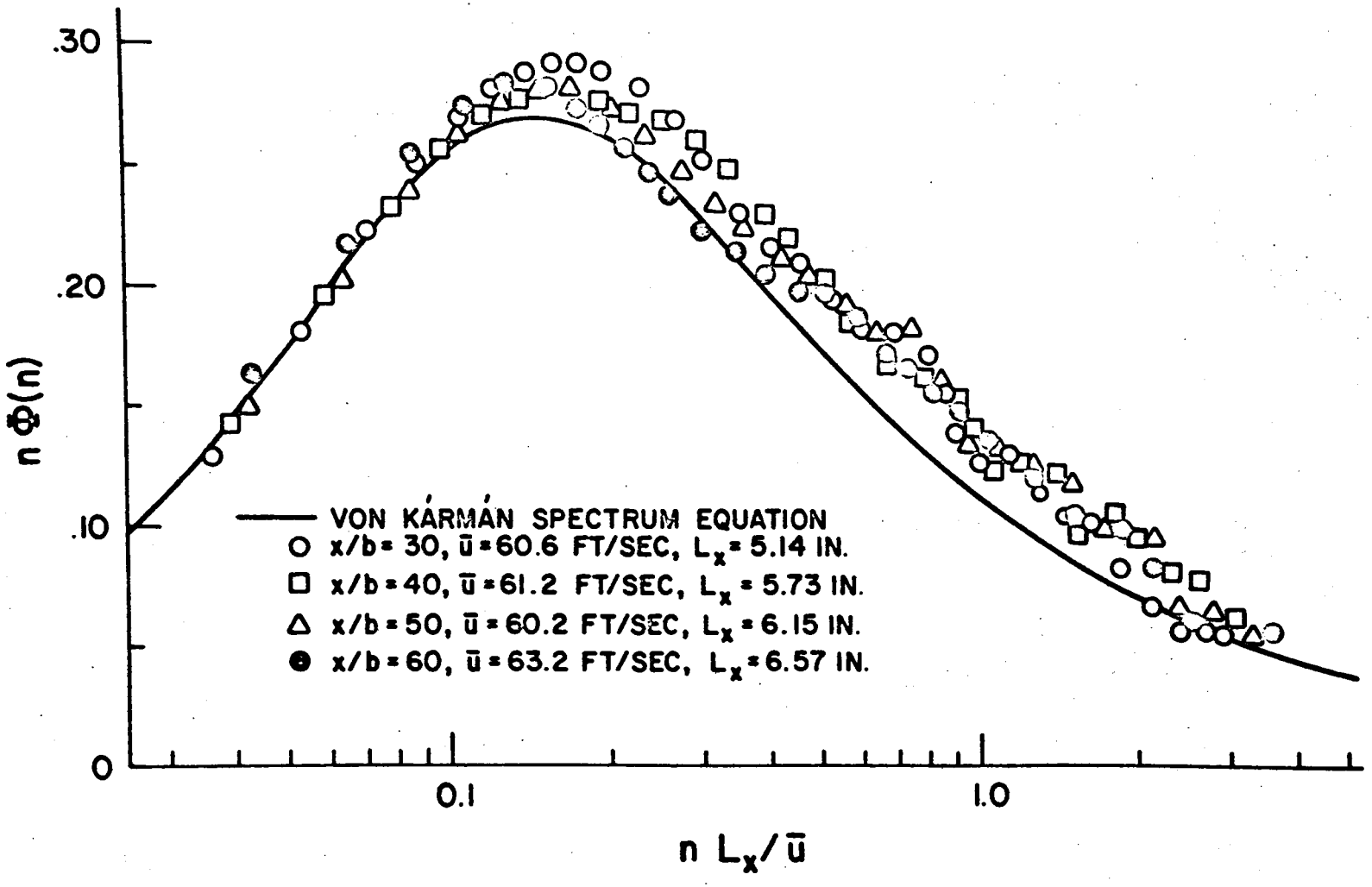

Figure 19: Improved estimates of power spectral density behind grid for $\bar{u} \approx 61.0$ ft./sec.

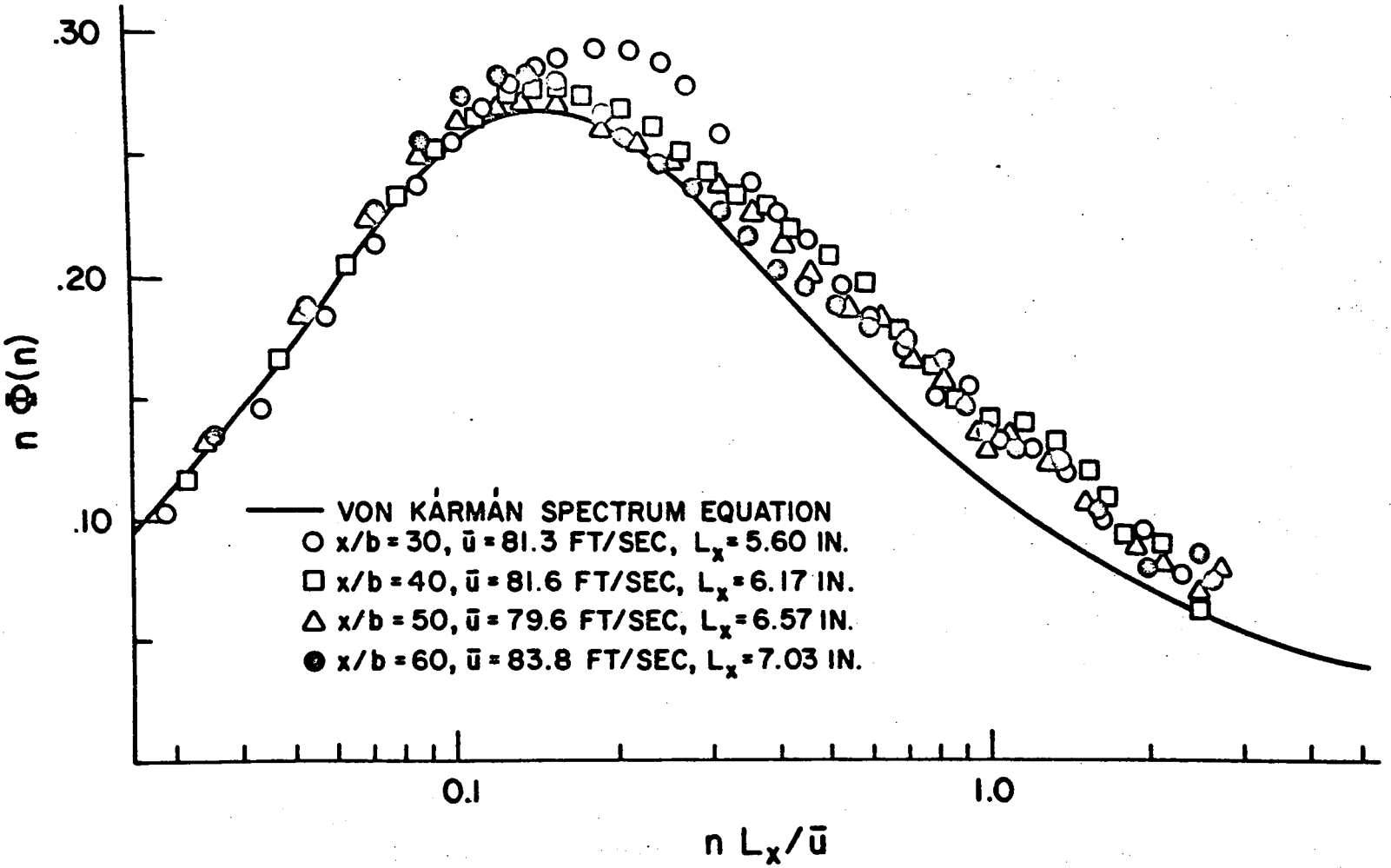

Figure 20: Improved estimates of power spectral density behind grid for $\bar{u} \approx 82.5$ ft./sec.

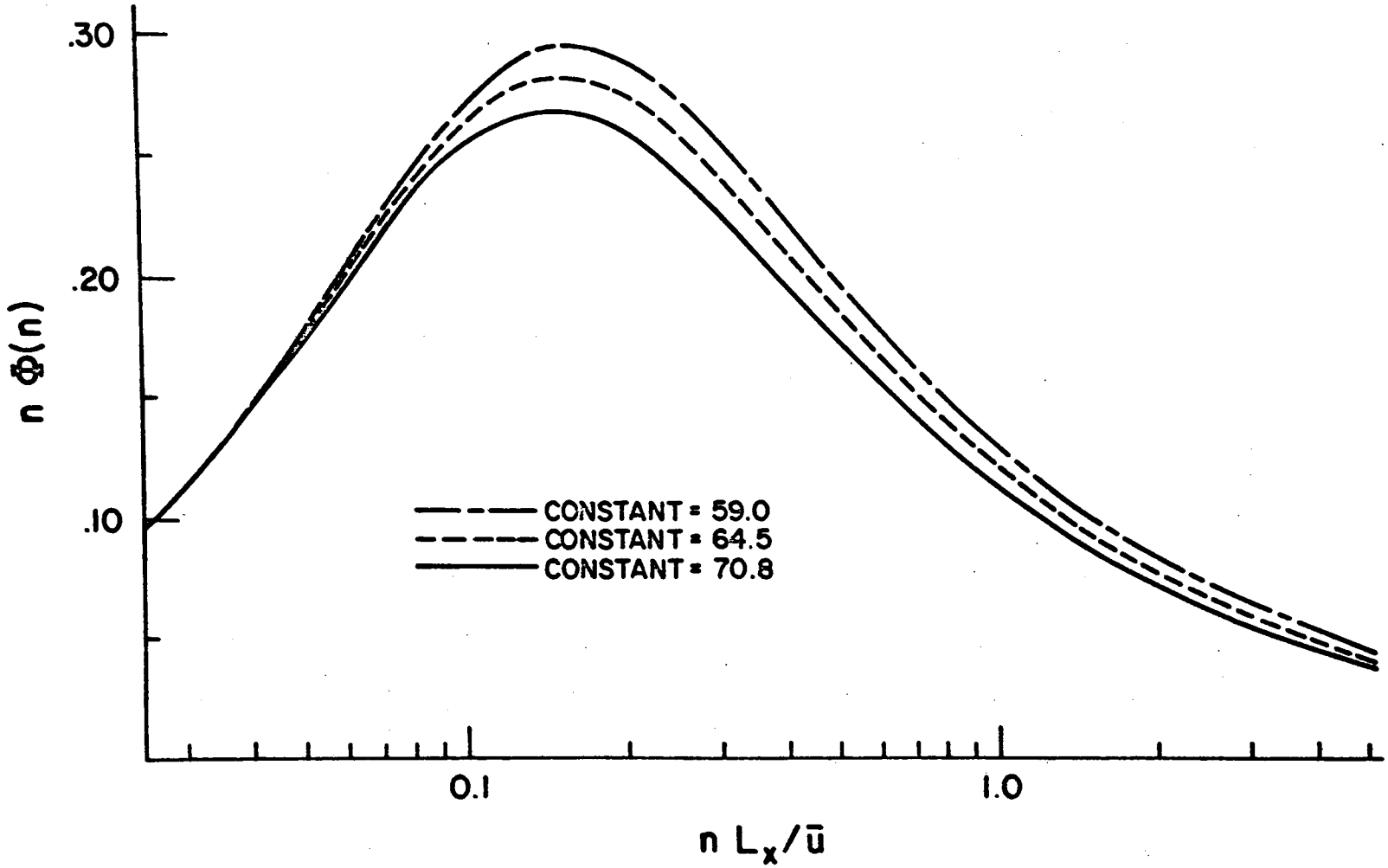

Figure 21: Von Karman spectrum equation for three values of the constant.

APPENDICES

APPENDIX A

DATA ACQUISITION

Experimental Apparatus

The experimental apparatus used in obtaining data for this study is quite simple. Two Pitot tubes and either one or two hot wire probes were mounted in the wind tunnel at a specific location downstream of the grid. One pitot tube and one hot wire were mounted on a traversing mechanism so that they were located at the same vertical position with a minimal horizontal separation. The wind velocity was set at a desired level by reference to the second Pitot tube which remained in the same position for all the tests. The traversing mechanism allowed the Pitot tube and probe to move vertically while the horizontal position remained unchanged. Thus the variations in wind velocity across the cross section of the tunnel could be measured. The second hot wire probe was used to measure the instantaneous wind velocity at a point near the center of the traverse of the moveable probe. The correlation coefficient between the signals of the two hot wire probes was determined for various vertical separations both above and below the location of the fixed probe.

Instrumentation

The instrumentation used in the tests included:

1. Two Disa type 55D01 Constant Temperature Anemometers
2. Two Disa type 55D35 RMS meters with variable capacitor time constants
3. One Disa type 55A06 Random Signal Indicator and Correlator

4. One Fluke Model 8200A digital volt meter with printer output unit.
5. A Barocel electronic manometer
6. A Precision Aneroid barometer
7. Two Tektronix AM 502 Differential amplifiers
8. A Honeywell model 5600B fourteen channel instrumentation tape recorder with FM cards.

The instrumentation networks used to obtain data are shown in Figures A-1 and A-2. Figure A-1 shows the configuration used in obtaining correlation coefficients between the two velocities and in obtaining turbulence intensity data. Figure A-2 shows the configuration used in obtaining a record of the instantaneous velocities at a point for subsequent statistical analysis.

Data Reduction

The velocity at a point in a turbulent flow can be considered as having a mean value and a fluctuating value. The determination of the velocity at a point can be performed by finding the mean and the fluctuating values separately. The mean velocity component was determined using a pitot static tube connected to the Barocel Electronic Manometer. The fluctuating velocity component was determined from the output of the hot wire anemometer. The anemometer output voltage varies in a nonlinear fashion with wind velocity. However, it was found that the logarithm of the output voltage varies linearly with the logarithm of the wind velocity for velocities

greater than 45 feet per second and linearly but with a different slope for velocities lower than 45 feet per second. A typical log-log plot of the probe voltage vs. wind velocity is shown in Figure A-3. There is some overlap of the curves between velocities of 40 and 50 feet per second. Figure A-4 shows the agreement of the calibration data with the calibration function generated from the least squares fit of the data for a typical probe. The slope of the calibration curve at a given wind velocity is required in order to calculate the variance and turbulence intensity of a velocity record. Though the probe output voltage varies nonlinearly with the velocity, it is assumed that the fluctuations in velocity about the mean velocity are small enough to allow a linear approximation in that region. Therefore the slope of the curve is taken to be a constant in that region and numerically equal to the slope of the calibration curve at the mean velocity. The probe output also varies with temperature but the slope of the calibration curve seems to be independent of temperature. In any event the operating temperature never differed by more than ten degrees from the calibration temperature. When calibration curves taken at two temperatures, differing by more than ten degrees, were used to calculate intensities and variances, the results differed by about one percent. By dividing the root mean square of the probe output voltage by the slope of the calibration curve at $\bar{u}$ equal to the mean velocity, the output is transformed from a voltage to a velocity measure, which is equal to the square root of the variance. The turbulence intensity is calculated by dividing the root mean square velocity by the mean velocity. Figure

A-5 shows a plot of the slope of a typical probe calibration curve for a range of velocities. The calibration curve is given by

$$E = c_1 \bar{u}^{c_2}.$$

The slope is found by differentiating the above equation with respect to the mean velocity.

$$\frac{dE}{d\bar{u}} = c_1 c_2 \bar{u}^{(c_2-1)}$$

Physical quantities calculated using this transformation are listed below.

Variance: $\overline{u^2} = \left| \frac{\text{R.M.S. voltage}}{c_1 c_2 \bar{u}^{(c_2-1)}} \right|^2$

Turbulence Intensity: $\frac{\sqrt{\overline{u^2}}}{\bar{u}} = \left| \left(\frac{\text{R.M.S. voltage}}{c_1 c_2 \bar{u}^{(c_2-1)}} \right) / \bar{u} \right|$

The computer program used to find the probe calibration function and then calculate the variance and turbulence intensity at specific points is listed on the next four pages.

```
C*****************************************************************************C
C                                                                             C
C     PROGRAM FIRST FINDS A FUNCTION TO FIT THE PROBE CALIBRATION DATA        C
C     ( LINES A-1 TO A-38 )  AND THEN DETERMINES THE TURBULENCE INTEN-        C
C     SITY AND THE VARIANCE FOR GIVEN POINTS  ( LINES A-39 TO A-55 )          C
C                                                                             C
C     THE LOG OF THE PROBE OUTPUT VOLTAGE AND THE LOG OF THE VELOCITY         C
C     ARE USED TO FIND THE BEST FIT TO A STRAIGHT LINE, IN THE LEAST          C
C     SQUARES SENSE                                                           C
C                                                                             C
C*****************************************************************************C
C                                                                             C
C                                INPUT  DATA                                  C
C                                                                             C
C     DELH  = HEAD : AS MEASURED FROM A PITOT TUBE IN INCHES OF WATER         C
C     PMB   = PRESSURE IN MILLIBARS                                           C
C     TEMP  = TEMPERATURE IN DEGREES FAHRENHEIT                               C
C     VOLT  = PROBE OUTPUT VOLTAGE                                            C
C     CONST = CONVERSION UNITS AND LUMPED CONSTANTS TO SATISFY                C
C             BERNOULLI'S EQUATION                                            C
C     RMS   = ROOT MEAN SQUARE OF PROBE VOLTAGE AT A POINT                    C
C     ZA    = VERTICAL POSITION OF PROBE                                      C
C     DIS   = POSITION OF PROBE DOWNSTREAM OF OBSTRUCTION                     C
C     L     = NUMBER OF POINTS                                                C
C                                                                             C
C*****************************************************************************C
C                                                                             C
C                              QUANTITIES GENERATED                           C
C                                                                             C
C     C1,C2,C3 = PROBE CALIBRATION CONSTANTS, FOR A GIVEN VELOCITY :          C
C                VOLT = C3 * ( VEL**C1 )                                      C
C     VEL   = THE AVERAGE VELOCITY                                            C
```

```
C       SA     = SLOPE OF CALIBRATION CURVE AT A SPECIFIC VELOCITY                C
C       XINT   = TURBULENCE INTENSITY                                             C
C       USQBR  = VARIANCE                                                         C
C                                                                                 C
C*****************************************************************************C
        DIMENSION SULA(20)                                                  A   1
        DIMENSION LABEL(20)                                                 A   2
        DIMENSION A(4), B(2)                                                A   3
        UX=0.0                                                              A   4
        VX=0.0                                                              A   5
        TY=0.0                                                              A   6
        UY=0.0                                                              A   7
        READ (5,12) LABEL                                                   A   8
        WRITE (6,13) LABEL                                                  A   9
        CONST=92.49214                                                      A  10
        READ , N                                                            A  11
        EN=N                                                                A  12
        WRITE (6,6)                                                         A  13
        DO 1 J=1,N                                                          A  14
        READ , DELH,PMB,TEMP,VOLT                                           A  15
        VEL=CONST*SQRT(DELH*(TEMP+460.0)/PMB)                               A  16
        X=ALOG(VEL)                                                         A  17
        Y=ALOG(VOLT)                                                        A  18
        WRITE (6,7) VEL,VOLT                                                A  19
        UX=UX+X**2                                                          A  20
        VX=VX+X                                                             A  21
        TY=TY+Y*X                                                           A  22
        UY=UY+Y                                                             A  23
1       CONTINUE                                                            A  24
        M=2                                                                 A  25
        IVPI=4                                                              A  26
        A(1)=UX                                                             A  27
```

```
      A(2)=VX                                                           A  28
      A(3)=VX                                                           A  29
      A(4)=EN                                                           A  30
      B(1)=TY                                                           A  31
      B(2)=UY                                                           A  32
      CALL SIMQ (A,B,M,KS,IVPI)                                         A  33
      C1=B(1)                                                           A  34
      C2=B(2)                                                           A  35
      C3=EXP(C2)                                                        A  36
      WRITE (6,8)                                                       A  37
      WRITE (6,9) C1,C2,C3                                              A  38
      DO 3 KL=1,3                                                       A  39
C     THIS LOOP ALLOWS ANALYSIS OF DATA FROM SEVERAL SETS OF DATA TAKEN    C
C     WITH THE SAME PROBE                                                  C
      READ (5,14) SULA                                                  A  40
      WRITE (6,15) SULA                                                 A  41
      WRITE (6,4)                                                       A  42
      READ , ZAZO,L,DIS                                                 A  43
      WRITE (6,5) DIS                                                   A  44
      WRITE (6,10)                                                      A  45
      DO 2 N=1,L                                                        A  46
      READ , DELH,PMB,ZA,TEMP,RMS                                       A  47
      ZA=ZA-ZAZO                                                        A  48
      VEL=CONST*SQRT(DELH*(TEMP+460.0)/PMB)                             A  49
      SA=C3*C1*(VEL**(C1-1))                                            A  50
      XINT=(RMS/SA)/VEL                                                 A  51
      USQBR=((RMS/SA)**2)                                               A  52
      WRITE (6,11) ZA,VEL,RMS,XINT,USQBR                                A  53
2     CONTINUE                                                          A  54
3     CONTINUE                                                          A  55
      STOP                                                              A  56
4     FORMAT (///,5X,19HHORIZONTAL POSITION,/)                          A  57
```

```
5     FORMAT (12X,F6.2)                                                A  58
6     FORMAT (///,8X,8HVELOCITY,8X,13HPROBE VOLTAGE,/)                 A  59
7     FORMAT (5X,E14.7,5X,E14.7)                                       A  60
8     FORMAT (//,11X,2HC1,17X,2HC2,17X,2HC3,/)                         A  61
9     FORMAT (3(5X,E14.7))                                             A  62
10    FORMAT (//,6X,12HVERTICAL POS,6X,13HMEAN VELOCITY,7X,11HRMS VOLTAG  A  63
     1E,9X,10HTURBULENCE,10X,5HUSQBR,/)                                A  64
11    FORMAT (5(5X,E14.7))                                             A  65
12    FORMAT (20A4)                                                    A  66
13    FORMAT (1H1,T10,20A4)                                            A  67
14    FORMAT (20A4)                                                    A  68
15    FORMAT (//,T10,20A4)                                             A  69
      END                                                              A  70
```

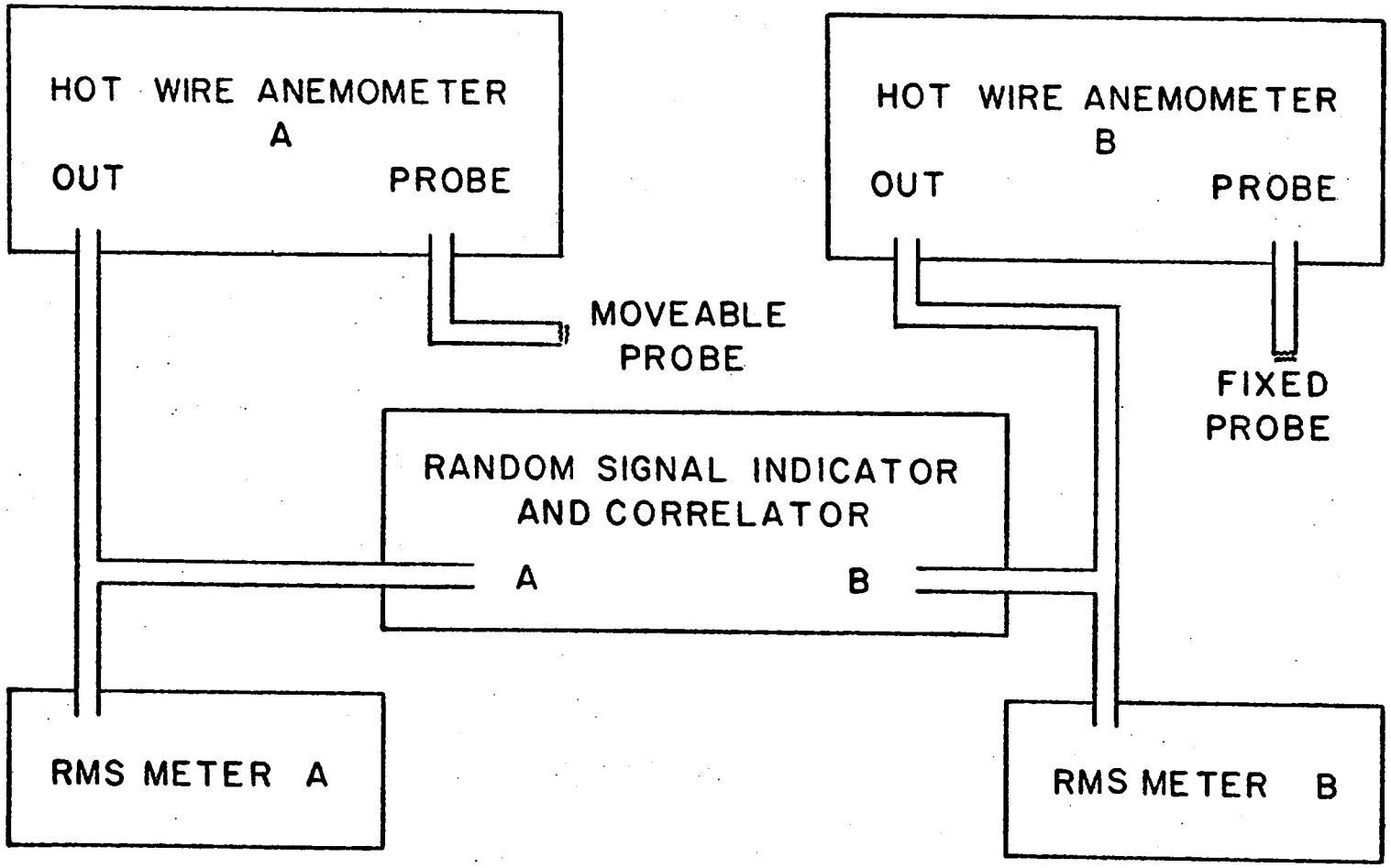

Figure A-1: Apparatus to Obtain Lateral Correlation Coefficient.

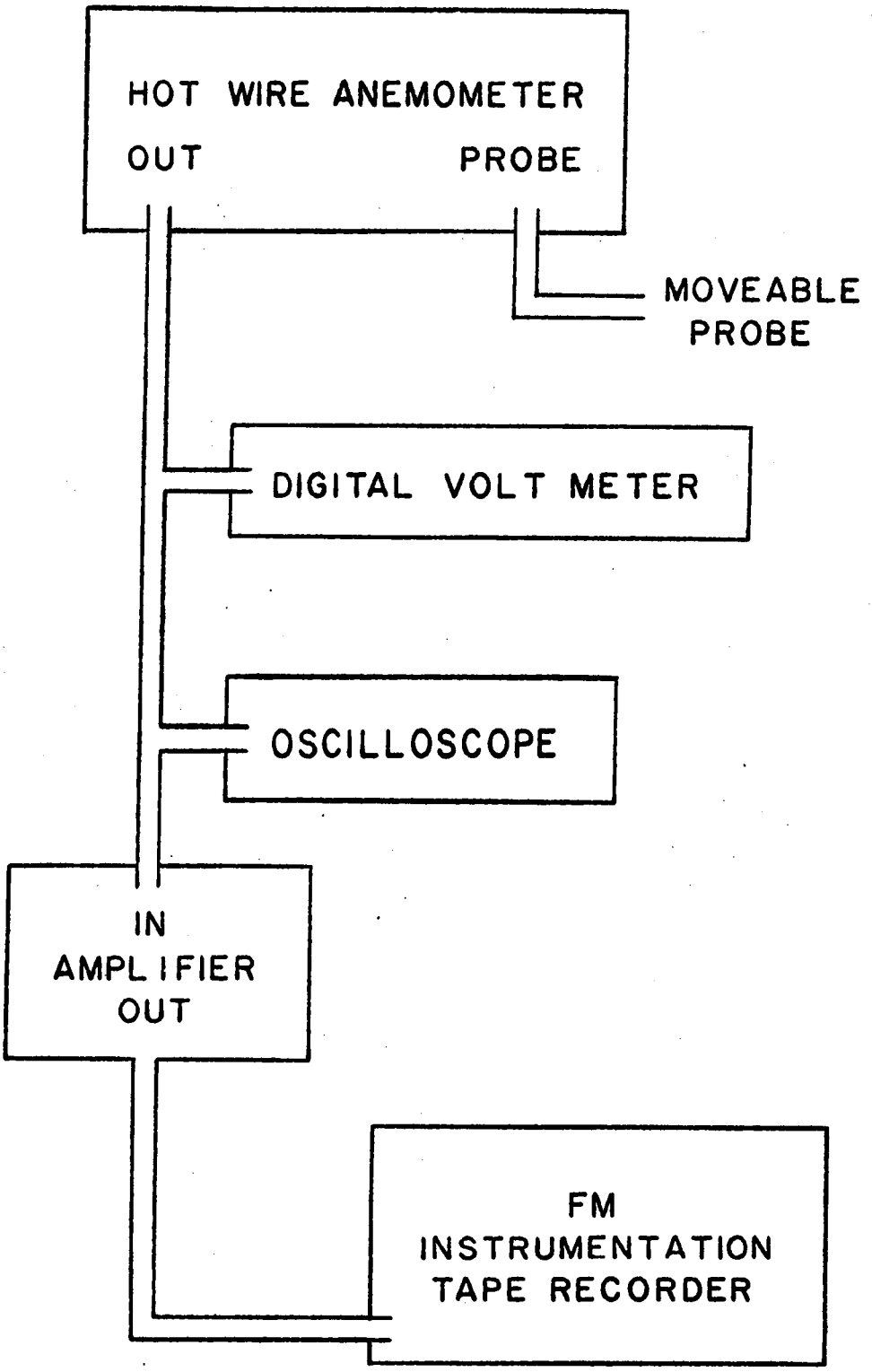

Figure 2-A: Apparatus to Obtain Velocity Record.

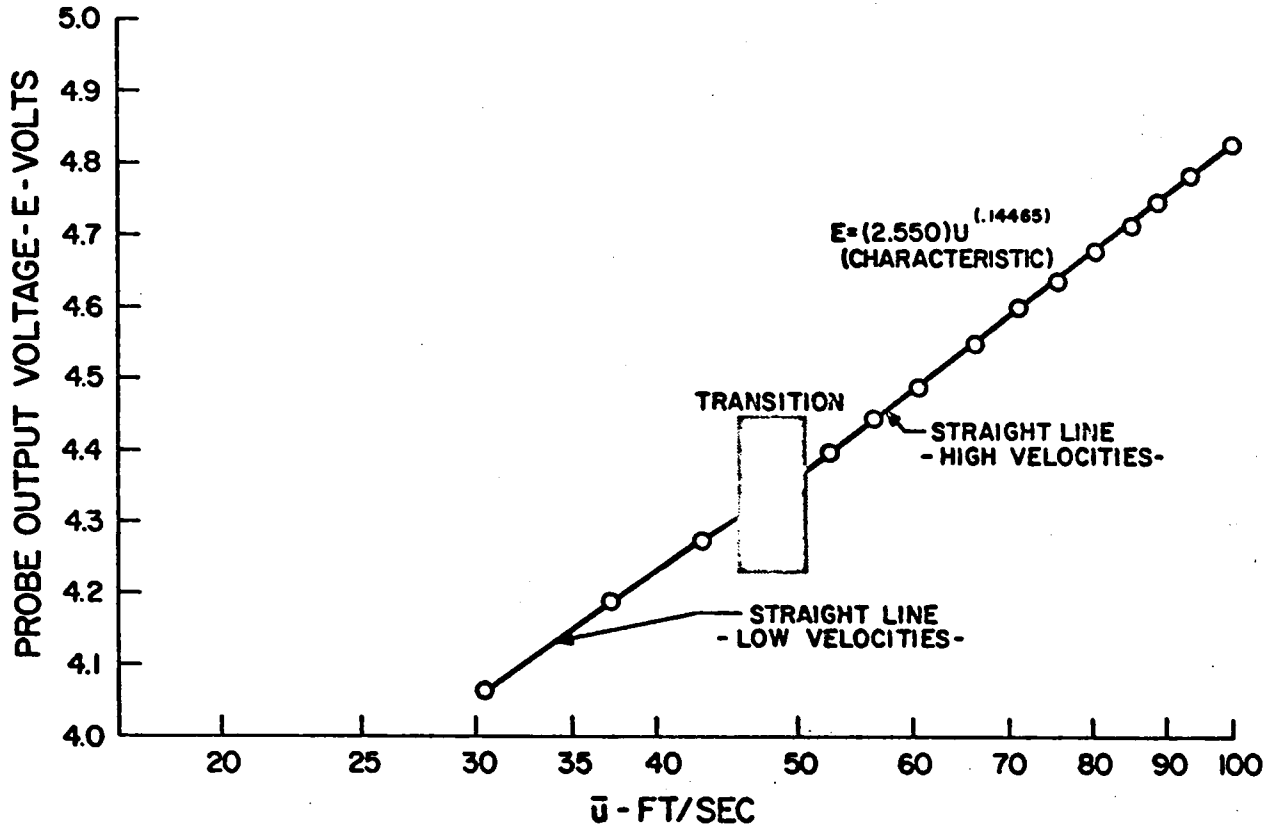

Figure A-3: Log-Log Plot of Prove Output Voltage Versus Wind Velocity.

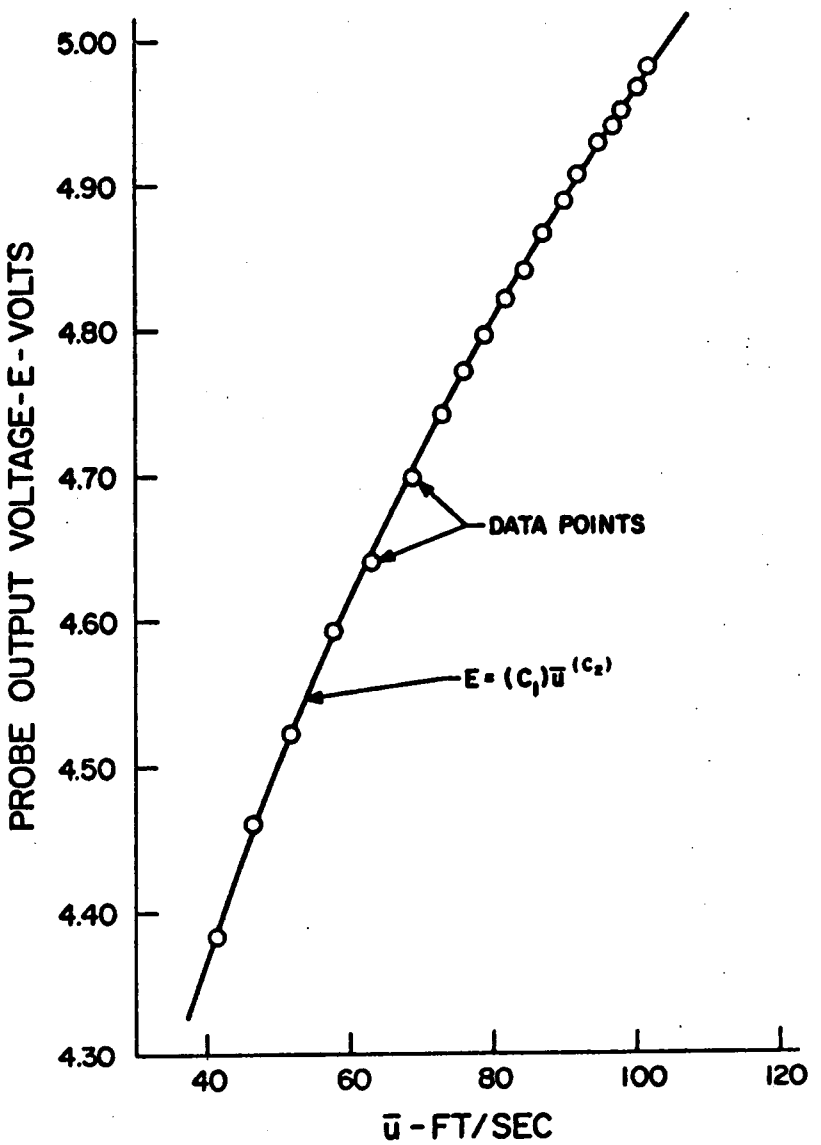

Figure A-4: Typical Probe Calibration Curve.

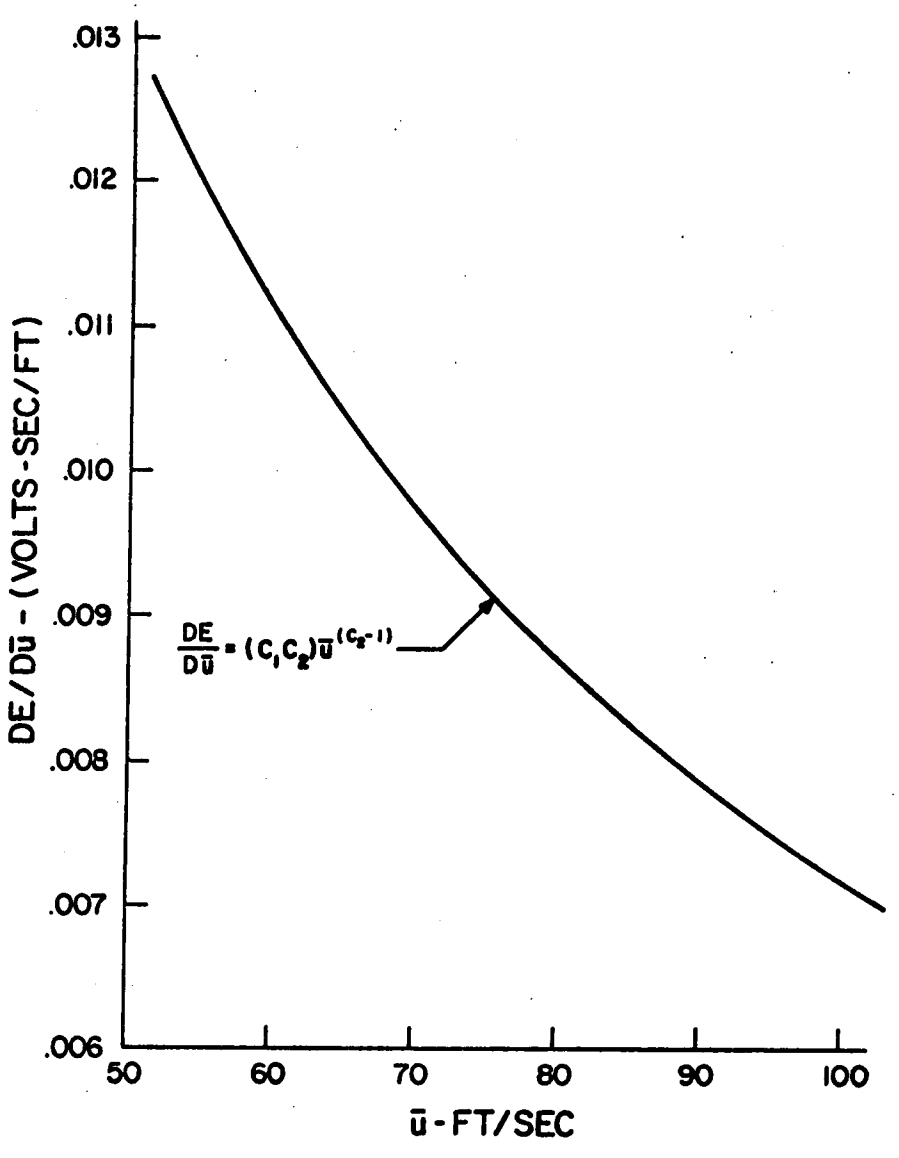

Figure A-5: Typical Plot of Slope of Calibration Curve.

APPENDIX B

CALCULATION OF STATISTICAL PROPERTIES OF THE FLOW

The description of a turbulent wind flow is only a rough sketch when the average properties are determined. The mean velocity, variance and turbulence intensity are such average measures which in a sense form a framework to which statistical properties add detail and depth. Appendix A describes the apparatus used to obtain data and the procedures used to calculate the average properties. Here, the discussion will focus on the methods of adding detail to the description of the flow by determination of the integral length scales and the power spectral density function.

The integral length scales are determined using the definition given in equations (2) and (5.1) in the text. The lateral integral length scale was found directly from the correlation coefficients which were determined while the tests were being performed (see Figure A-1 in Appendix A). The correlation coefficients were plotted versus the lateral separation of the probes. The area under the curve is proportional to the lateral integral length scale. The longitudinal integral length scale was determined using the autocorrelation function. By use of Taylor's hypothesis the time correlation multiplied by the mean velocity is equivalent to a spatial correlation. The top portion of Figure B-1 shows the equipment configuration used to generate the autocorrelation function. The integral length scales represent a characteristic dimension of the eddies in the flow. Since the flow is close to being isotropic and because of the symmetry of the flow

the lateral integral length scale is the characteristic dimension in the Y-Z plane, the cross sectional plane of the tunnel. Both integral length scales can be thought of as the principal dimensions of the characteristic large scale energy containing eddies.

The key element in finding the integral length scale and the power spectral density function of the longitudinal velocity component, is the autocorrelation function of a longitudinal velocity record. A single hot wire probe placed in the tunnel with its filament perpendicular to the flow measures the longitudinal velocity component with negligible influence of the lateral velocity components. The probe output was recorded using the equipment configuration shown in Figure A-2. The mean velocity was determined independently of the hot wire probe and the only portion of the velocity needed for statistical analysis was the fluctuating component. The mean voltage was removed prior to recording by use of an AC coupled amplifier with a 3 db. down low frequency roll off of two cycles per second. This also allowed the best use of the tape recorder since the signal could be amplified for accurate reproduction of the fluctuating component without exceeding the range of the recorder. The frequency range of velocity fluctuations which was of interest for structural response of the bridge models was between five cycles per second and one hundred cycles per second. Thus velocity records were made using a tape speed of one and seven eights which has a frequency response up to about 600 cycles per second. The low pass filter on the amplifier was set for a 3 db. down frequency roll off of 500 cycles per second. If 500Hz is considered to be the highest

frequency present in the signal, the minimum sampling rate to avoid aliasing must be 1,000 samples per second. The delay range on the correlator was set so that the delay time between correlations was 0.5 milliseconds which corresponds to 2,000 samples per second. This delay range was such that the correlation function decayed to zero before the end of the one hundred point autocorrelation function. Additional consecutive sets of one hundred points could be generated by using the pre-computational delay. The longer correlation record used to determine the effects of the finite correlation record length was created using the pre-computational delay.

The power spectral density function was calculated by performing a Fourier transformation of the autocorrelation curve. Figure B-1 shows the possible methods of communicating the autocorrelation function to the IBM 370 for power spectral density function calculation. The Program used to calculate the power spectral density estimate and the improved estimate, as described in the text, is listed on the next six pages.

```
C*****************************************************************************C
C                                                                             C
C            PROGRAM FOR CALCULATING POWER SPECTRAL DENSITY FUNCTION          C
C              FROM AUTOCORRELATION CURVE OF WIND VELOCITY RECORD             C
C                                                                             C
C*****************************************************************************C
C                                                                             C
C                                INPUT  DATA                                  C
C                                                                             C
C  FIRST CARD                                                                 C
C     C1 AND C3 = PROBE COEFFICIENTS FROM LEAST SQUARES FIT OF CALIBRA-       C
C                 TION CURVE USING A LOG-LOG STRAIGHT LINE APPROXIMATION      C
C  SECOND CARD                                                                C
C     LABL   = FOUR CHARACTER ALPHA - NUMERIC LABEL FOR DATA POINT            C
C     TEMP   = TEMPERATURE IN DEGREES FAHRENHEIT                              C
C     DELH   = HEAD :  MEASURED BY PITOT TUBE AT THE PROBE LOCATION           C
C     RMS    = THE ROOT MEAN SQUARE OF THE PROBE VOLTAGE                      C
C  THIRD CARD                                                                 C
C     DETAILED LABEL IDENTIFYING DATA, POSITION OF PROBE AND DATE             C
C  FOURTH CARD                                                                C
C     LAG    = NUMBER OF AUTOCORRELATION CURVE DATA POINTS                    C
C              ( VALUES OF R(T) )                                             C
C     DT     = SIZE OF TIME INCREMENTS                                        C
C     HSHIFT= CONSTANT DC VOLTAGE OFFSET OF CORRELATOR OUTPUT                 C
C  CARDS  5 - (LAG/10)                                                        C
C     AUTOCORRELATION CURVE DATA POINTS                                       C
C  LAST CARD                                                                  C
C     X      = DISPLACEMENT DOWNSTREAM OF GRID                                C
C                                                                             C
C*****************************************************************************C
C                                                                             C
C                             QUANTITIES GENERATED                            C
```

```
C                                                                       C
C     UBAR   = THE AVERAGE VELOCITY                                     C
C     DEDU   = THE SLOPE OF THE PROBE CALIBRATION CURVE                 C
C     USQB   = THE VARIANCE                                             C
C     W(K)   = WINDOW SHAPEING FUNCTION USED IN OBTAINING P.S.D.F.      C
C              ESTIMATE                                                 C
C     ACVF(I) = VALUES OF AUTOCORRELATION FUNCTION SCALED TO PHYSICAL   C
C                QUANTITIES                                             C
C     WF(I) = FOURIER TRANSFORM OF THE WINDOW FUNCTION W(K)             C
C     FLXW   = FREQUENCY * LONG. INTEGRAL LENGTH SCALE / MEAN VELOCITY  C
C     SPECK = FIRST ESTIMATE OF P.S.D.F. FROM FOURIER TRANSFORM OF      C
C              AUTOCORRELATION CURVE                                    C
C     VSPEC = NORMALIZED FIRST ESTIMATE OF P.S.D.F.                     C
C     SN     = P.S.D.F. FROM VON KARMAN EQUATION WITH CONST. = 70.78    C
C              FROM EQUATION (14) IN TEXT                               C
C     SNW    = NORMALIZED P.S.D.F. FROM VON KARMAN EQUATION             C
C     GN     = NORMALIZED ESTIMATE OF SN BASED ON CONVOLUTION OF SN     C
C              WITH WF, EQUATION (12) IN TEXT                           C
C     PERC   = DIFFERENCE BETWEEN SNW AND GN DIVIDED BY GN  ( CORRECTION C
C              FACTOR TO REMOVE GROSS EFFECTS OF USE OF THE PARTICULAR  C
C              WINDOW FROM THE P.S.D.F. ESTIMATE )                      C
C     VNSPEC= IMPROVED ESTIMATE OF P.S.D.F. BASED ON FOURIER TRANSFORM  C
C              OF THE AUTOCORRELATION CURVE                             C
C                                                                       C
C***********************************************************************C
      DIMENSION H(201), ACVF(201), W(201), FREQ(201), WF(60), LABEL(20),   A   1
     1 F(60)
      READ (5,12) C1,C3                                                   A   3
      CK=C1-1.0000000                                                     A   4
      READ (5,13) LABL,TEMP,PMB,DELH,RMS                                  A   5
      WRITE (6,10) LABL,C1,C3,TEMP,PMB,DELH,RMS                           A   6
      UBAR=92.449*SQRT(((TEMP+460.0)*DELH)/PMB)                           A   7
```

```
      DEDU=C3*C1*UBAR**CK                                               A   8
      USQB=(RMS/DEDU)**2                                                A   9
      READ (5,18) (LABEL(I),I=1,20)                                     A  10
      READ (5,15) LAG,DT,HSHIFT                                         A  11
      WRITE (6,14) LAG,DT,HSHIFT                                        A  12
      WRITE (6,19) (LABEL(I),I=1,20)                                    A  13
C*********************************************************************C
C                        CALCULATION OF WINDOW FUNCTION                C
C*********************************************************************C
      NTRUNK=LAG-1                                                      A  14
      X=LAG                                                             A  15
      PI=3.14159                                                        A  16
      DO 1 K=1,NTRUNK                                                   A  17
      P=K                                                               A  18
      W(K)=0.5*(1.0+COS(PI*P/X))                                        A  19
1     CONTINUE                                                          A  20
      READ (5,16) (H(I),I=1,LAG)                                        A  21
C*********************************************************************C
C                            REMOVAL OF DC OFFSET                      C
C*********************************************************************C
      DO 2 I=1,LAG                                                      A  22
      H(I)=H(I)-HSHIFT                                                  A  23
      ACVF(I)=(H(I)/H(1))*USQB                                          A  24
2     CONTINUE                                                          A  25
      WRITE (6,17) (H(I),I=1,LAG)                                       A  26
C*********************************************************************C
C                                                                       C
C             CALCULATION OF FOURIER TRANSFORM OF WINDOW FUNCTION       C
C                                                                       C
C     F   = FREQUENCY AT WHICH WINDOW FUNCTION TRANSFORM IS CALCULATED  C
C     DEF = INCREMENT IN FREQUENCY                                      C
C                                                                       C
```

```
C     THE WINDOW FUNCTION TRANSFORM IS CALCULATED AT THIRTY VALUES OF        C
C     THE FREQUENCY ON EITHER SIDE OF THE CENTER FREQUENCY                   C
C                                                                            C
C*************************************************************************C
      F(1)=0.0                                                          A  27
      DEF=1.0                                                           A  28
      DO 6 I=1,30                                                       A  29
      SUM=0.0                                                           A  30
      DO 3 J=1,NTRUNK                                                   A  31
      SUM=SUM+2.0*W(J)*COS(2.0*PI*F(I)*J*DT)                            A  32
3     CONTINUE                                                          A  33
      IF (I.GT.1) GO TO 4                                               A  34
      WF(30)=(W(1)+SUM)*DT                                              A  35
4     CONTINUE                                                          A  36
      IF (I.EQ.1) GO TO 5                                               A  37
      WF(29+I)=(W(1)+SUM)*DT                                            A  38
      WF(31-I)=WF(29+I)                                                 A  39
5     CONTINUE                                                          A  40
      F(I+1)=F(I)+DEF                                                   A  41
6     CONTINUE                                                          A  42
C*************************************************************************C
C                CALCULATION OF LONGITUDINAL INTEGRAL LENGTH SCALE          C
C                          FROM EQUATION (9.5) IN TEXT                      C
C*************************************************************************C
      READ , X                                                          A  43
      ALX=(0.55*3.6*ALOG(X)+0.022*UBAR-5.46)/12.0                       A  44
      WRITE (6,11) UBAR,USQB,ALX                                        A  45
      WRITE (6,21)                                                      A  46
C*************************************************************************C
C
C                 CALCULATION OF POWER SPECTRAL DENSITY FUNCTION            C
C                                                                            C
```

```
C       NPTPLT = NUMBER OF POINTS AT WHICH P.S.D.F. WILL BE CALCULATED          C
C       FREQ   = FREQUENCY AT WHICH P.S.D.F. IS CALCULATED, 'N' IN HZ           C
C       DELX   = INCREMENT IN FREQUENCY                                         C
C                                                                               C
C*******************************************************************************C
C       FREQ(1) = INITIAL FREQUENCY AT WHICH P.S.D.F. IS CALCULATED          A  47
        NPTPLT=180                                                           A  48
        FREQ(1)=2.5                                                          A  49
        DELX=2.5                                                             A  50
        DO 9 M=1,NPTPLT                                                      A  51
C*******************************************************************************C
C        CALCULATION OF FIRST ESTIMATE OF POWER SPECTRAL DENSITY FUNCTION       C
C*******************************************************************************C
        SUMM=0.0                                                             A  52
        DO 7 K=1,NTRUNK                                                      A  53
        L=K+1                                                                A  54
        SUMM=SUMM+2.0*ACVF(L)*W(K)*COS(2.0*PI*FREQ(M)*K*DT)                  A  55
7       CONTINUE                                                             A  56
        SPECK=2.0*(ACVF(1)+SUMM)*DT                                          A  57
C*******************************************************************************C
C                    CONVOLUTION OF VON KARMAN EQUATION WITH WF                 C
C*******************************************************************************C
        FO=FREQ(M)-29.0                                                      A  58
        SUMM=0.0                                                             A  59
        FQ=FO                                                                A  60
        DO 8 L=1,59                                                          A  61
        FQ=FQ+DEF                                                            A  62
        FA=ABS(FQ)                                                           A  63
        SN=(4.00*USQB*ALX/UBAR)/((1.0+70.78*((ALX*FA/UBAR)**2))**.833333)    A  64
        SUMM=SUMM+(SN*WF(L)*DEF)                                             A  65
8       CONTINUE                                                             A  66
C*******************************************************************************C
```

```
C          CALCULATION OF IMPROVED POWER SPECTRAL DENSITY FUNCTION          C
C*****************************************************************************C
      FE=FREQ(M)                                                          A  67
      GN=FE*SUMM/USQB                                                     A  68
      SN=(4.00*USQB*ALX/UBAR)/((1.0+70.78*((ALX*FE/UBAR)**2))**.833333)   A  69
      SNW=SN*FE/USQB                                                      A  70
      PERC=(SNW-GN)/GN                                                    A  71
      VSPEC=SPECK*FREQ(M)/USQB                                            A  72
      VNSPEC=VSPEC+VSPEC*PERC                                             A  73
      FLXW=FREQ(M)*ALX/UBAR                                               A  74
      WRITE (6,20) VSPEC,FREQ(M),VNSPEC,FLXW,SNW,PERC,GN                  A  75
      FREQ(M+1)=FREQ(M)+DFLX                                              A  76
9     CONTINUE                                                            A  77
      STOP                                                                A  78
10    FORMAT (10X,6HTEST: ,A4,//10X,19HPROBE COEFFICIENTS:,5X,5HC1 = ,F1  A  79
     10.7,5X,5HC3 = ,F10.7,//10X,7HTEMP = ,F6.2,5X,6HPMB = ,F7.2,5X,7HDE  A  80
     2LH = ,F5.2,5X,6HRMS = ,F7.4,/)                                      A  81
11    FORMAT (//,10X,16HMEAN VELOCITY = ,F8.3,5X,32H(RMS INSTANT. VELOCI  A  82
     1TY) ** 2  = ,F8.3,5X,6HALX = ,F12.7)                                A  83
12    FORMAT (5X,F10.7,2X,F10.7)                                          A  84
13    FORMAT (A4,6X,F6.2,4X,F7.2,4X,F5.2,4X,F7.4)                         A  85
14    FORMAT (10X,19HNUMBER OF POINTS = ,I6,5X,8HDELAY = ,F10.5,5X,12HDC  A  86
     1 OFFSET = ,F9.5,/)                                                  A  87
15    FORMAT (2X,I6,2X,F8.5,2X,F7.4)                                      A  88
16    FORMAT (10F7.4)                                                     A  89
17    FORMAT (10X,10F7.4)                                                 A  90
18    FORMAT (20A4)                                                       A  91
19    FORMAT (25X,20A4)                                                   A  92
20    FORMAT (7(5X,F12.7))                                                A  93
21    FORMAT (///,10X,5HVSPEC,11X,6HFREQ=N,11X,6HVNSPEC,10X,9HN*LX/UBAR,  A  94
     1 11X,3HSNW,13X,4HPERC,14X,2HGN,/)                                   A  95
      END                                                                 A  96
```

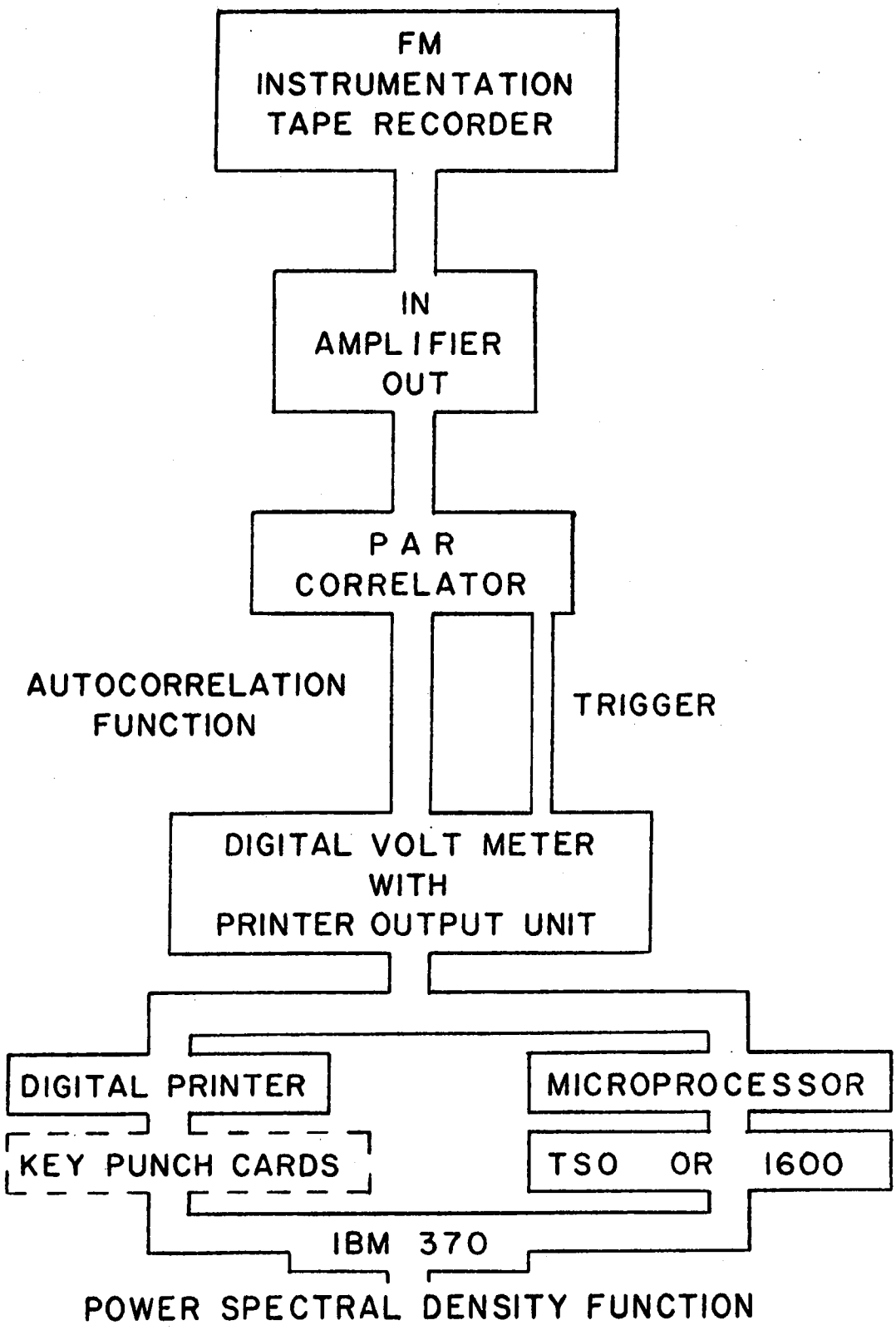

Figure B-1: Flow chart of analysis of velocity record.

The vita has been removed from the scanned document

INVESTIGATION OF A GRID INDUCED TURBULENT ENVIRONMENT FOR WIND TUNNEL TESTING

by

Timothy Allen Reinhold

(ABSTRACT)

In performing wind tunnel model tests of a two-dimensional nature, a grid constructed of 3.6 x 0.75 inch boards on 18 inch centers was used at the entrance of the tunnel. Important properties of the turbulent flow behind the uniform coarse grid were determined. The flow was found to be quite uniform at a distance of 38 bar widths downstream of the grid. Use of this flow to simulate atmospheric turbulent flows for testing sectional models of suspension bridges is discussed. The power spectra of the turbulence was found to agree quite well with the von Karman spectrum equation for atmospheric turbulence. The integral length scales were found to increase with increasing distance downstream of the grid. Integral length scales of the longitudinal turbulence component were found to increase in size as the mean velocity was increased. Measurements indicate that grid turbulence seems to model the atmospheric turbulence quite well for studies of suspension bridges and other elevated structures. Meaningful quantitative results may be obtained if geometric modeling of the integral length scales of the atmospheric turbulence is of minor importance for proper model response.